

Definition and calculation of bottom quark cross-sections in deep-inelastic scattering at HERA and determination of their uncertainties

Tancredi Carli,^a Vincenzo Chiochia^{bcd} and Katarzyna Klimek^c

^a*EP Division, CERN, 1211 Geneva, Switzerland*

^b*DESY, Notkestr. 85, 22607 Hamburg, Germany*

^c*University of Hamburg, Luruper Chaussee 149, 22607 Hamburg, Germany*

^d*Physik Institut der Universität Zürich-Irchel, 8057 Zürich, Switzerland*

E-mail: Tancredi.Carli@cern.ch, Vincenzo.Chiochia@cern.ch, kklimek@mail.desy.de

ABSTRACT: The uncertainties involved in the calculation of bottom quark (b -quark) cross-sections in deep-inelastic scattering at HERA are studied in different phase space regions. Besides the inclusive b -quark cross-section, definitions closer to the detector acceptance requiring at least one high energetic muon from the semi-leptonic b -quark decay or a jet with high transverse energy are investigated. For each case the uncertainties due to the choice of the renormalisation and factorisation scales as well as the b -quark mass are estimated in the perturbative NLO QCD calculation and furthermore uncertainties in the fragmentation of the b -quark to a B -meson and in its semi-leptonic decay are discussed.

KEYWORDS: Lepton-Nucleon Scattering.

Contents

1. Introduction	1
2. Leading order QCD Monte Carlo simulation programs	3
3. Measurement and definition of bottom quark cross-sections	4
4. Perturbative LO and NLO QCD calculations and fragmentation models	6
4.1 Perturbative LO and NLO QCD cross-section calculations	7
4.2 Fragmentation of the b -quark	7
4.3 The semi-leptonic decay of the B -meson into a muon and a jet	10
5. Comparison of the leading order calculations	11
6. Perturbative NLO QCD calculations and their uncertainties	13
6.1 Calculated NLO QCD cross-sections	13
6.2 Factorisation and renormalisation scale and b -quark mass uncertainties	14
6.3 Parton density uncertainties	21
6.4 Fragmentation function uncertainties	23
7. QCD model uncertainties	24
7.1 Extrapolations uncertainties due to QCD models	24
7.2 Hadronisation corrections uncertainties	27
8. Conclusions	28

1. Introduction

Quantum Chromodynamics (QCD) has proven to give a correct description of the strong interaction, if a hard scale is involved in the process such that perturbation theory is applicable. The large charm (c) and especially the bottom (b) quark mass (m_b) provide such a hard scale, since $m_b \gg \Lambda$, where $\Lambda \approx 250 \text{ MeV}$ is the typical QCD scale. The large mass screens the collinear singularities, so that there is no need to apply a jet algorithm or to subtract them into a fragmentation function in the perturbative cross section calculation. Non-perturbative contributions to heavy quark momentum distributions are of order $\mathcal{O}(\Lambda/m_b)$. The production of bottom quarks should therefore be well described by perturbative QCD calculations, but the inclusion of non-perturbative effects is unavoidable to get a physically complete result.

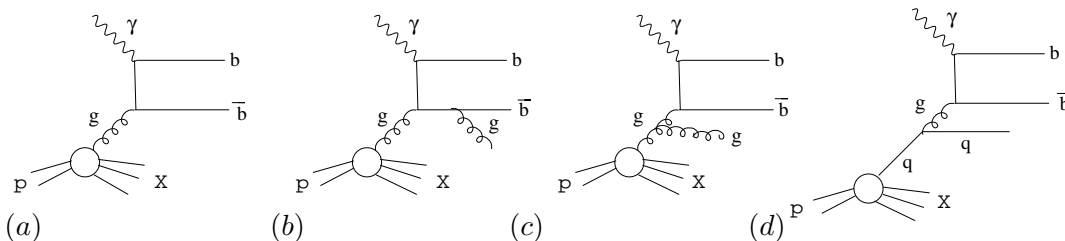


Figure 1: (a) Leading order Feynman diagram for the reaction $\gamma p \rightarrow b\bar{b}X$, (b c d) some generic Feynman diagrams of the $\mathcal{O}(\alpha_s^2)$ contributions.

The b -quark production cross-sections in strong interactions have been measured in proton-antiproton collisions at SPS [1] and at Tevatron [2]–[8] and, more recently, in two-photon interactions at LEP [9] and in photon-proton collisions (γp) at the electron-proton (ep) collider HERA [10, 11]. For all these measurements, except the early SPS data [1], the measured b -quark production cross-sections lie above perturbative QCD expectations calculated up to next-to-leading order (NLO) in the strong coupling, α_s . Since the production of bottom quarks is an important background process in searches for phenomena beyond the Standard Model at present and future high energy colliders, the understanding of the observed excess of the measurement over the perturbative QCD expectation, has recently been lively discussed. Possible proposed solutions involve higher order effects estimated by resummation of large logarithms [12, 13], new parton evolution schemes [14, 15, 16], fragmentation effects [17] or even the exchange of low-mass supersymmetric particles [18]. Meanwhile the last possibility seems to be excluded from LEP data [19].

Deep-inelastic scattering (DIS) offers the unique opportunity to study the production mechanism of bottom quarks in a particularly clean environment where a point-like projectile, a virtual photon (γ^*), collides with a proton. It will be interesting to see, if the excess observed in photoproduction [10, 11], where the photon is real and can develop a hadronic structure, persists for virtual photons. The large centre-of-mass energy of HERA colliding 27.5 GeV electrons on 920 GeV protons allows a sufficient number of $b\bar{b}$ pairs to be produced and provides therefore an excellent and clean testing ground.

The calculation of the b -quark production cross-section requires the knowledge of the parton densities (mainly the one of the gluon), of the perturbatively calculable hard parton parton subprocess and the correct modeling of the long range effects binding the b -quark in the hadrons. The Feynman diagram of the basic production mechanism for the reaction $\gamma^* p \rightarrow b\bar{b}X$ is sketched in leading order (LO) of the strong coupling $\mathcal{O}(\alpha_s)$ in figure 1a. As examples some generic Feynman diagrams of the NLO contributions are shown in figure 1b–d. The dominant process is the fusion of the virtual photon emitted by the electron with a gluon from the proton. The production of b -quarks is therefore directly sensitive to the gluon density in the proton. Furthermore the gluon evolution can be tested in the presence of several possible hard scales like m_b , the photon virtuality Q^2 or the transverse energy of the jet initiated by the bottom quark.

A recent theoretical review on the NLO QCD calculation of heavy quark cross-section in DIS can be found in [20].

In this paper we investigate the uncertainties involved in the calculation of the bottom quark production cross-section in DIS for different cross-section definitions and we address the question how the calculations can be best compared to experimental results: a short description of the perturbative NLO QCD calculation based on the HVQDIS program [21, 22, 23], the model of the fragmentation of the b -quark in a B -meson and its semi-leptonic decay to a muon and a jet. Tools to simulate b -quark production are described in section 2. After a short overview of the experimental techniques to identify bottom quarks, different cross-section definitions based on the measurable quantities: the scattered electron, the muon from the semi-leptonic b -quark decay and the jet initiated by the b -quark are presented in section 3. Section 4 presents the necessary elements needed for the calculation of the cross-section for the reaction $ep \rightarrow b\bar{b} \rightarrow e\mu jet X$. The LO QCD calculation based on HVQDIS is compared to the LO QCD models Monte Carlo simulations in section 5. The uncertainties involved in the NLO QCD cross-section calculations are discussed in section 6. This includes the uncertainties of the factorisation and the renormalisation scales, the b -quark mass, the parton densities, the phenomenological description of the fragmentation process and other non-perturbative effects. In addition, the uncertainties involved in extrapolating the measurable cross-section $ep \rightarrow b\bar{b} \rightarrow e\mu jet X$ to a more inclusive cross-section like e.g. $ep \rightarrow b\bar{b} \rightarrow eX$ are discussed in section 7.

2. Leading order QCD Monte Carlo simulation programs

QCD Monte Carlo models are able to simulate the hadronic final state of a DIS event in full detail. The four-momenta of all produced particles are made explicitly available. These programs are indispensable tools to correct the experimental data for detector effects. Although they only contain the leading order matrix elements of the hard subprocess, they include higher orders in a leading logarithmic approximation and they make use of models providing detailed treatment of the non-perturbative fragmentation phase. Here, there are mainly used to test the simple fragmentation model implemented in the NLO QCD calculation and to study the uncertainty of extrapolating measured cross-section to more inclusive ones. Another purpose is to study possible effects from higher orders implemented in the leading logarithm approximation.

The RAPGAP Monte Carlo [24] incorporates the $\mathcal{O}(\alpha_s)$ QCD matrix elements (ME) and approximates higher order parton emission using the concept of parton showers (PS) [25] based on the leading logarithm DGLAP equations [26, 27, 28]. QCD radiation can occur before and after the hard subprocess. The formation of hadrons is simulated using the LUND string model [29] as implemented in JETSET [30]. As an option parton showers can also be simulated using ARIADNE [31]. In this model gluon emissions are treated by the colour dipole model [32, 33] (CDM) assuming a chain of independently radiating dipoles spanned by colour connected partons.

In the CASCADE Monte Carlo simulation program [34] higher order parton emissions based on the CCFM [35]–[38] evolution equations are matched to a $\mathcal{O}(\alpha_s)$ matrix element [39]–[42], where the incoming parton can be off-shell. The CCFM evolution equations are based on k_T -factorisation and angular ordering which is a consequence of colour coher-

ence, i.e. due to the interference properties of the radiated gluons. As a result in the appropriate limit they reproduce the DGLAP [26, 27, 28] and the BFKL [43, 44, 45] approximation. At small values of the parton momentum fractions z , a random walk of the transverse parton momenta k_T is obtained. The CCFM evolution is based on k_T -factorisation [46], where the partons entering the hard scattering matrix element are free to be off-shell, in contrast to the collinear approach (DGLAP) which treats all partons entering the hard subprocess as massless. Off-shell matrix elements of heavy flavour lepto- and hadroproduction processes have been calculated in ref. [46]. The unintegrated gluon density¹ used in CASCADE is extracted through a fit to the proton structure function F_2 measured at HERA [47]. The fit was performed in the range $x < 10^{-2}$ and $Q^2 > 5 \text{ GeV}^2$. Recently, it has been shown that CASCADE is able to correctly reproduce the b -quark production cross-section in $p\bar{p}$ -collisions at Tevatron [14].

In all calculations no QED corrections have been included.

3. Measurement and definition of bottom quark cross-sections

When a b -quark with high transverse energy is produced in a hard strong interaction, a jet can be measured in the final state. The jet is composed by a hadron containing the b -quark (in most cases a B -meson) and other hadrons produced in the fragmentation process. Due to the large b -quark mass the jet is expected to be wider than a jet at similar transverse energy initiated by a light quark. However, since the rate of b -quarks is much smaller than the one of light quarks, this characteristic feature is not sufficient to clearly identify the presence of a b -quark. Therefore usually the semi-leptonic decay modes of the B -meson to electrons and to muons $B \rightarrow eX$ and $B \rightarrow \mu X$ are exploited to identify the presence of a b -quark. This largely suppresses the background from the light quarks u , d and s , which basically only can fake such a signature when a hadron produced in a light quark jet is misidentified as an electron or muon. The remaining background from charm quarks can be statistically separated from the b -quark signal, since the lifetime of the meson containing the charm quark and the kinematics of the meson decay is significantly different. This is due to the smaller charm mass. In many cases the analysis of the muon channel is experimentally easier than the one of the electron channel. Therefore, here we only refer to the muon channel.²

The experimental method often relies on the measurement of the transverse momentum (P_T^{rel}) of the muon produced in the semi-leptonic decay relative to the jet axis. Due to the higher b -quark mass the spectrum of this quantity is harder for jets initiated by b -quarks than by charm quarks. When this method is used, a jet and a muon have to be measured. Complementary information can be obtained from lifetime measurements of the B -meson with the help of high precision silicon vertex detectors. A particularly elegant and

¹Unintegrated means that the gluon density depends on the transverse parton momenta emitted along the cascade. This dependence is not integrated out as in the DGLAP approach where the gluon density only depends on the energy fraction x and on the squared transverse momentum transfer.

²All the arguments are, of course, also valid for semi-leptonic decays into electrons.

simple method measures only the impact parameter³ of the muon track with respect to the main interaction vertex. Therefore, in principle in this method only a muon is needed to extract the b -quark production cross-section. An alternative b -quark tag can be obtained via the identification of a D^* -meson. This method gives access to low b -quark momenta, but is not considered here, since the efficiency of this method is rather low.

Besides the presence of the scattered electron the experimental definition of a b -quark cross-section in DIS therefore requires the presence of a muon with typically a momentum bigger than a few GeV and/or the presence of a jet associated to the muon at high transverse energy in the detector. The b -quark cross-section measurements should always be quoted for the reaction $ep \rightarrow e\mu(jet)X$.

To circumvent a complex cross-section definition, to facilitate the evaluation of the NLO QCD calculation and to make a comparison between different experimental results easier, in the past often extrapolations of the experimentally measured cross-section to a more inclusive definition have been made using leading order QCD Monte Carlo simulation programs. Such a procedure can only be adopted, if the models used for the extrapolation is reliable. Since in many cases the involved extrapolations are large, it is doubtful whether the accuracy of the leading order QCD Monte Carlo simulation programs is sufficient. In any case, unnecessary model uncertainties are introduced in the experimental cross-section measurement which, when not properly stated, can make the direct comparison of data very difficult, if the extrapolation have been based on different model assumptions.⁴

Besides the experimentally required cross-section definition for the reaction $ep \rightarrow b\bar{b} \rightarrow e\mu jetX$ ($\sigma_{b,jet,muon}$), in this paper we will investigate the total inclusive b -quark cross-section only defined by the scattered electron measured in the detector (σ_b), the b -quark cross-section where in addition a hard jet is measured ($\sigma_{b,jet}$) and the b -quark cross-section where a muon, but no hard jet is required ($\sigma_{b,muon}$).

The scattered electron should be well measured in the main part of the detector. Therefore we require that the minimal Q^2 of the exchanged photon should be $Q^2 > 2 \text{ GeV}^2$. Since with the present HERA data sample very high Q^2 values are not accessible, Q^2 is restricted to $Q^2 < 1000 \text{ GeV}^2$. The quantity $y = Q^2/(sx)$, where $x = Q^2/(2Pq)$ is the Bjorken scaling variable, q (P) is the four-momentum of the exchanged photon (the proton beam) and s is the squared centre-of-mass energy, is set to $0.05 < y < 0.7$. The lower cut on y ensures that the squared invariant mass of the hadronic final state $W^2 = (q+P)^2 = ys$ is large enough to produce a final state with high transverse energy. The higher cut on y is needed to ensure a good reconstruction of the event kinematics and to suppress non-DIS background.⁵

The jet should be well inside the acceptance of the calorimeter and the muon well inside the acceptance of the muon chambers and the inner tracking detectors. We require

³The impact parameter is the distance of closest approach of the muon track to the primary event vertex. The average impact parameter measured in the laboratory frame is directly related to the lifetime of the B -meson in its rest frame.

⁴This is almost always the case, if older data are compared to recent ones.

⁵High values of y correspond to low energies of the scattered electron where the unambiguous identification of the scattered electron becomes more difficult.

	DIS	JET	MUON
Symbol	$2 < Q^2 < 1000 \text{ GeV}^2$ $0.05 < y < 0.7$	$E_{T,\text{jet,Breit}} > 6 \text{ GeV}$ $-2 < \eta_{\text{jet,lab}} < 2.5$	$P_{\mu,\text{lab}} > 2 \text{ GeV}$ $30^\circ < \theta_\mu < 160^\circ$
σ_b	x		
$\sigma_{b,\text{jet}}$	x	x	
$\sigma_{b,\text{muon}}$	x		x
$\sigma_{b,\text{jet,muon}}$	x	x	x

Table 1: Definition of the b -quark production cross-sections used in this analysis. For each definition the applied cut is marked with the symbol x .

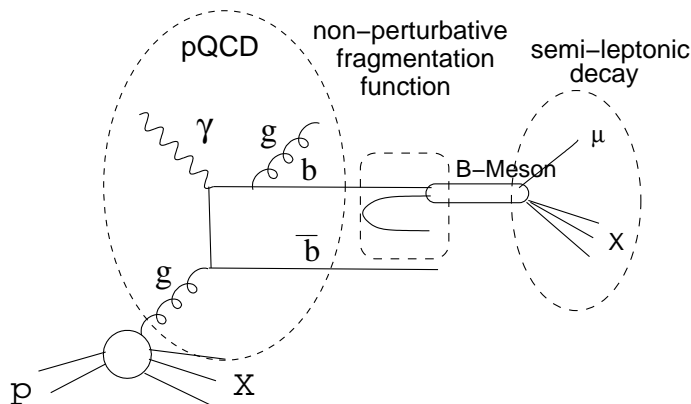


Figure 2: Sketch of the production of a B -meson in DIS and its subsequent decay.

here $-2 < \eta_{\text{jet,lab}} < 2.5$ and $30^\circ < \theta_{\mu,\text{lab}} < 160^\circ$ which corresponds to $-1.7 < \eta_{\mu,\text{lab}} < 1.3$. When the muon should be identified in the muon chambers it needs a sufficiently large momentum to penetrate the calorimeters. In our case we consider $P_{\mu,\text{lab}} > 2 \text{ GeV}$.

A hard interaction is signaled by the presence of a jet with high transverse energy. The jet definition is based on the inclusive k_T -algorithm [48, 49]. To cluster particles or partons to jets the E_T scheme is used. The resulting jet four-momentum is therefore massless. This algorithm is well suited to make quantitative comparisons with NLO calculation, since it is infra-red and collinear safe [50]. To remove the purely kinematic dependence of the transverse jet energy on the photon virtuality Q^2 , the transverse jet energy is measured in a frame where the photon and the proton collide head on. Such a frame is e.g. the Breit frame defined by $2x\vec{P} + \vec{q} = 0$. A jet with a transverse energy $E_{T,\text{jet,Breit}} > 6 \text{ GeV}$ is required in the Breit frame. The jet should be within the detector acceptance. We require here: $-2 < \eta_{\text{jet,lab}} < 2.5$.

The different cross-section definitions are summarised in table 1.

4. Perturbative LO and NLO QCD calculations and fragmentation models

The b -quark cross-section measurements often rely on the identification of a muon from the semi-leptonic decay of a B -meson. To be comparable to the measurements the calculation of the b -quark cross-section proceeds in three steps as it is illustrated in figure 2:

1. The perturbative QCD calculation of the hard parton parton scattering cross-section convoluted with the parton densities and the strong coupling for the reactions $ep \rightarrow b\bar{b}$, $ep \rightarrow b\bar{b}g$ and $ep \rightarrow b\bar{b}q$
2. The fragmentation of the b -quark into a B -meson described by a non-perturbative fragmentation function
3. The semi-leptonic decay of the B -meson into a muon and hadrons.

4.1 Perturbative LO and NLO QCD cross-section calculations

The NLO QCD heavy quark cross-sections for DIS can be calculated using the HVQDIS program [21, 22, 23]. For each event all contributions of the reactions $ep \rightarrow b\bar{b}$, $ep \rightarrow b\bar{b}g$ and $ep \rightarrow b\bar{b}q$ are evaluated. Since the four-momenta of the outgoing particles are made explicitly available, the single and double differential distributions as well as correlations among all outgoing particles can be studied. Furthermore HVQDIS allows to easily apply experimental cuts.

The b -quark production cross-section in ep scattering can be expressed as a product of the strong coupling, the parton densities and the hard scattering parton cross-section which can be expanded in a series of perturbatively calculable coefficient functions including the matrix elements and the phase space factors. While the total ep b -quark cross-section is a well defined physical quantity which can be compared to experimental data, the individual terms depend on the used calculation scheme.

The divergences of the coefficient functions calculated to the order $\mathcal{O}(\alpha_s^2)$ due to soft gluon emissions are compensated by contributions from virtual gluon exchange using the subtraction method. The renormalisation is carried out in the modified minimal subtraction scheme (\overline{MS}) for light quarks. The divergences from heavy quark loops are subtracted such that the heavy quark mass only enters in the coefficient functions. In the energy evolution of the strong coupling and in the evolution of the parton densities equations only light quarks appear. The CTEQ5F4 [51] parameterisation of the parton densities is used as default. In this parameterisation the number of active quark flavours in the proton is fixed to four. As default, the mass of the b -quark is set to $m_b = 4.75$ GeV. The uncertainty on this value is assumed to be ± 0.25 GeV.

Uncertainties in the perturbative calculations are due to the choice of the renormalisation (μ_r^2) and the factorisation (μ_f^2) scales and due to the uncertainties on the b -mass. In addition the uncertainty on the parton densities, in particular the gluon density, contributes. The uncertainty on the parton density function is evaluated using the ZEUS NLO QCD fit to recent measurements of the proton structure function [52].

4.2 Fragmentation of the b -quark

The fragmentation of the b -quark into a B -meson is a non-perturbative process. It can be described by a fragmentation function obtained from comparisons with data. The fragmentation of b -quarks has recently been carefully studied in e^+e^- collisions using weakly decaying B -mesons [53]–[57]. Several fragmentation functions describing the distribution of the b -quark energy fraction carried by the B -meson have been tested and parameterisa-

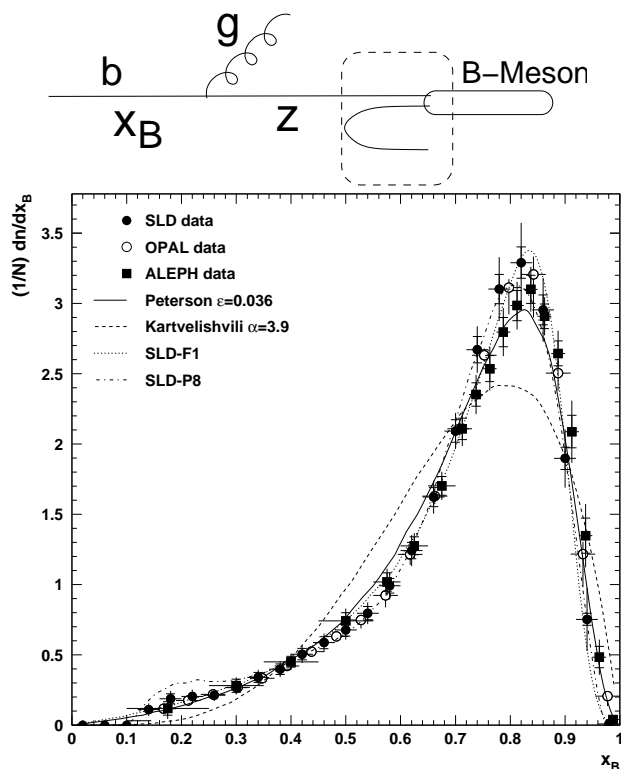


Figure 3: Shape of the distribution of the energy fraction $x_B = 2E_B/\sqrt{s}$ carried by the B -meson with respect to the energy of the b -quark measured in e^+e^- collisions. Shown are data together with some selected fragmentation function parameterisations (see text).

tions which describe the data best have been provided. Since in e^+e^- collisions the initial energy of the b -quark is known, they are usually parameterised as a function of the ratio of the B -meson energy (E_B) and the beam energy (E_{beam}) which corresponds to the energy of the b -quark :

$$x_B = \frac{E_B}{E_{\text{beam}}} = \frac{2E_B}{\sqrt{s}}, \quad (4.1)$$

where \sqrt{s} is the centre-of-mass energy of the collision. The variable x_B can be interpreted as the fraction of the b -quark energy which is carried by the B -meson .

The b -quark fragmentation functions as a function of x_b measured by the SLD, OPAL and ALEPH collaborations are shown in figure 3 together with some selected parameterisations [57, 58, 59]. The data have been measured at a centre-of-mass energy which corresponds to the mass of the Z^0 -boson. They are consistent with each other. The parameterisations based on phenomenological models are roughly able to reproduce the data.

However, the energy fraction of the b -quark just before entering the fragmentation process, i.e. the b -quark energy fraction after additional parton emissions, is not experimentally accessible (see also the sketch on top of figure 3). The knowledge of the distribution of this variable, called z in the following, is, however, necessary to make predictions for B -meson production cross-sections in other reactions.⁶

⁶In HVQDIS z is defined as $\vec{p}_B = z\vec{p}_b$, where \vec{p}_b (\vec{p}_B) is the momentum of the b -quark (B -meson).

The fragmentation function $f(z)$ can in principle be obtained from the B -meson cross-section by folding them with the b -quark production cross-section (σ_b):

$$\sigma_B \propto \int \sigma_b(z, \mu_{\text{FF}}^2, \dots) f(z, \mu_{\text{FF}}^2) dz, \tag{4.2}$$

where μ_{FF}^2 is the factorisation scale which determines which contributions should be absorbed in the perturbative part and which in the non-perturbative fragmentation process. The separation between the pQCD calculation and the fragmentation function is arbitrary, parts of the calculable contributions can be absorbed in the fragmentation function and vice versa. When evaluating the physically observable B -meson cross-section the perturbative and the non-perturbative part have to be carefully matched to each other. In this sense the extracted fragmentation function always depends on the scheme how the perturbative cross-section σ_b has been calculated. As a consequence, when applying the fragmentation function $f(z)$ for cross-section predictions in a different reaction, care has to be taken that the same approximations are applied in the perturbative calculation. In praxis, this can be quite tricky, since in a different reaction different parts of the perturbative calculation, like e.g. resummations of logarithms etc., might have to be taken into account. Since in e^+e^- collisions at LEP or at the SLAC linear collider the centre-of-mass energy is usually much larger than the b -quark mass, in the perturbative calculable part large logarithms of the form $\log(s/m_b^2)$ have to be resummed (NLL) [60]. It is not clear that such contributions also have to be included for the cross-section calculations in $p\bar{p}$ -collisions or DIS. Here, rather a resummation of terms $\log(E_{T,b}^2/m_b^2)$, where $E_{T,b}$ is the b -quark transverse energy, is needed [12, 61].

As default, we follow the suggestion in refs. [17, 62] to use fragmentation functions where the fourth Mellin moment, defined as $f_N = \int_0^1 z^{N-1} f(z) dz$ with $N = 4$, folded with a perturbative NLL calculation is in agreement with the e^+e^- data. Such a procedure is optimal when the calculations are compared to data which exhibit a cross-section behaviour like $d\sigma_b/dE_{T,b} \propto 1/dE_{T,b}^4$, which is the case in b -quark production at Tevatron as well as in DIS at HERA for large transverse momenta of the b -quark (see line in figure 6).⁷ The parameterisation of Kartvelishvili et al. [59], $f(x, \alpha) = (\alpha + 1)(\alpha + 2)x^\alpha(1 - x)$ is proposed [17, 62], since it is consistent with an expansion in powers of λ/m_b , where $\lambda \approx 0.4$ is a typical hadronic scale, as it is predicted by QCD [63, 64, 65]. The parameter⁸ $\alpha = 27.5$ is obtained from a fit to the ALEPH data [17, 55, 62]. The perturbative part has been calculated to NLO accuracy together with a resummation of logarithmic terms to all orders. It is not clear whether such a resummation is also needed for the range of $E_{T,b}$ presently accessible in DIS at HERA.

Therefore and also since the spectrum of the transverse b -quark momentum deviates from the power-law behaviour (see above) at low values, one can use different parame-

⁷The reason is that then in the moment space the b -quark cross-section is just given as product of $1/E_{T,b}^n$ and the n th-moment of the fragmentation function $f_N(z)$, since $d\sigma_b/dE_{T,b} \propto \int dz d\hat{E}_{T,b} f(z) \frac{1}{E_{T,b}^n} \delta(z\hat{E}_{T,b} - E_{T,b}) = \frac{1}{E_{T,b}^n} f_N(z)$.

⁸Note, that this value for α is quite different than the one best describing the $(1/N)dn/dx_b$ distributions, namely $\alpha = 3.9$ [57], which is shown in figure 3.

terisations with different adjustable parameters to investigate the uncertainty due to the fragmentation function. As alternative e.g. the parameterisation⁹ of Peterson et al. [58] can be used.

4.3 The semi-leptonic decay of the B -meson into a muon and a jet

After the B -meson is produced it decays via a charged current interaction. In some cases the B -meson decays semi-leptonically, e.g. a muon and a jet is produced. The muon can either be produced by a direct semi-leptonic decay ($B \rightarrow \mu X$) or by an indirect decay where the b -quark decays first to a charm quark which subsequently decays semi-leptonically to a muon ($B \rightarrow cX \rightarrow \mu X$). About 10% of all B -meson decays are direct decays into muons, in 8% (2%) of the cases the muons are indirectly produced by a charm (anti-charm) decay. Other decay modes of the b -quark are much smaller, e.g. $B \rightarrow J/\psi X \rightarrow \mu X$ is approximately $7 \cdot 10^{-4}$ and $B \rightarrow \tau X \rightarrow \mu X$ is $\approx 7 \cdot 10^{-3}$. The branching fractions presently implemented in JETSET agree within 3% with the measured ones. The agreement in the different channels is reasonable. In the HVQDIS calculation the cross-section is determined using the sum of the branching ratios of direct and indirect decays of the B -meson¹⁰ decays into a muon is $\mathcal{B}_\mu = 0.22$.

In the calculation of the cross-section $ep \rightarrow b\bar{b} \rightarrow \mu X$ it has to be taken into account that the measured muon can stem from the b -quark or the \bar{b} -quark. For this purpose, it is assumed that the b -quark and the \bar{b} -quark are both independently decaying into muons according to the branching ratio \mathcal{B}_μ . We ignore the case where a b -quark produces two muons via $b \rightarrow c\mu X \rightarrow \mu\mu X$. If one of the muons is in the detector acceptance, the event is counted in the calculation. To improve the efficiency of the calculation, one can as an alternative always decay one of the b -quarks in a muon and then decay the other one according to the probability that exactly two muons are in the event under the condition that there is at least one muon, i.e. $P_{2\mu \geq 1\mu} = \mathcal{B}_\mu^2 / (2\mathcal{B}_\mu - \mathcal{B}_\mu^2) = \mathcal{B}_\mu / (2 - \mathcal{B}_\mu)$. The cross-section has then to be multiplied with the probability that there is at least one muon $P_{\geq 1\mu} = 1 - (1 - \mathcal{B}_\mu)(1 - \mathcal{B}_\mu) = 2\mathcal{B}_\mu - \mathcal{B}_\mu^2$. To ensure the cancellation of the different divergences appearing in the NLO QCD calculation care has to be taken that for one event defined, e.g. by a common x and Q^2 value, only one common z -value is used for the different contributions appearing in a NLO QCD calculation.

To correctly model the kinematics of the muon decay a parameterisation of the muon momentum spectrum in the centre-of-mass frame of the B -meson is needed. Since the muon spectrum for direct ($B \rightarrow \mu X$) and indirect ($B \rightarrow cX \rightarrow \mu X$) B -meson decays is different, the correct mixture has to be used. Muons are generated isotropically in the rest frame of the B -meson. The absolute momentum p is obtained with the help of a probability function extracted from the muon momentum spectrum as obtained from JETSET. Figure 4 shows

⁹The explicit form is: $N \frac{1}{z} (1 - \frac{1}{z} - \frac{\epsilon}{1-z})^{-2}$, where N is a normalisation factor and ϵ is an adjustable parameter, which should be in the order of $\epsilon = m^2/M_B^2 \approx 0.002$, where m (M_B) is a typical mass of a light (B) meson. Note, that the value $\epsilon = 0.002$ is a crude estimation and not a result of a fit to the data.

¹⁰The term B -meson refers here to the mixture used in JETSET, i.e. $0.4025 B^0 + 0.4025 B^+ + 0.094 B_s + 0.101 \Lambda_b$. This mixture is in agreement with the data [66]: $(0.38 \pm 0.13) B^0 + (0.388 \pm 0.13) B^+ + (0.106 \pm 0.13) B_s + (0.118 \pm 0.2) \Lambda_b$.

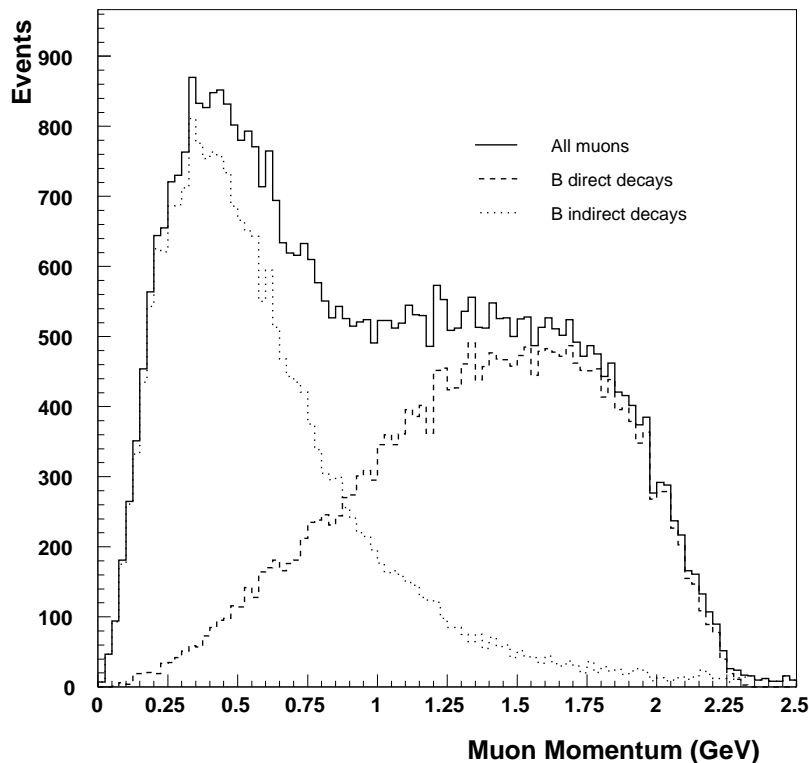


Figure 4: Momentum distribution of the decay muons in the rest frame of the parent B -meson. The contributions from direct ($b \rightarrow \mu X$) and indirect ($b \rightarrow cX \rightarrow \mu X$) decays are shown separately.

the muon momentum distribution in the rest frame of the B -meson, dN/dp . The total distribution is shown as solid line, the distributions corresponding to the direct and indirect B -decays are shown as dashed and dotted lines separately. The direct B -meson decays produce events with higher muon momenta.

5. Comparison of the leading order calculations

To check that the simple form of b -quark fragmentation and of the subsequent decay of the B -meson implemented in HVQDIS gives reasonable results, a comparison to the more complex fragmentation models used in the Monte Carlo simulation programs can be made. For this purpose, the same free parameters in the perturbative cross-section calculations have to be chosen. A comparison of the LO QCD prediction of the inclusive DIS b -quark cross-section calculated by HVQDIS and by RAPGAP¹¹ is shown in figure 5. The renormalisation and factorisation scale $\mu^2 = \mu_f^2 = \mu_r^2 = Q^2$ has been used and the b -quark mass was set to $m_b = 5 \text{ GeV}$. Moreover the 1-loop formula of the strong coupling α_s and the CTEQ5L parton density functions have been used.

¹¹To obtain a pure LO calculation in RAPGAP, the parton shower option has been switched off. Moreover, for the calculation of the differential b -quark and jet cross-section the fragmentation has been switched off.

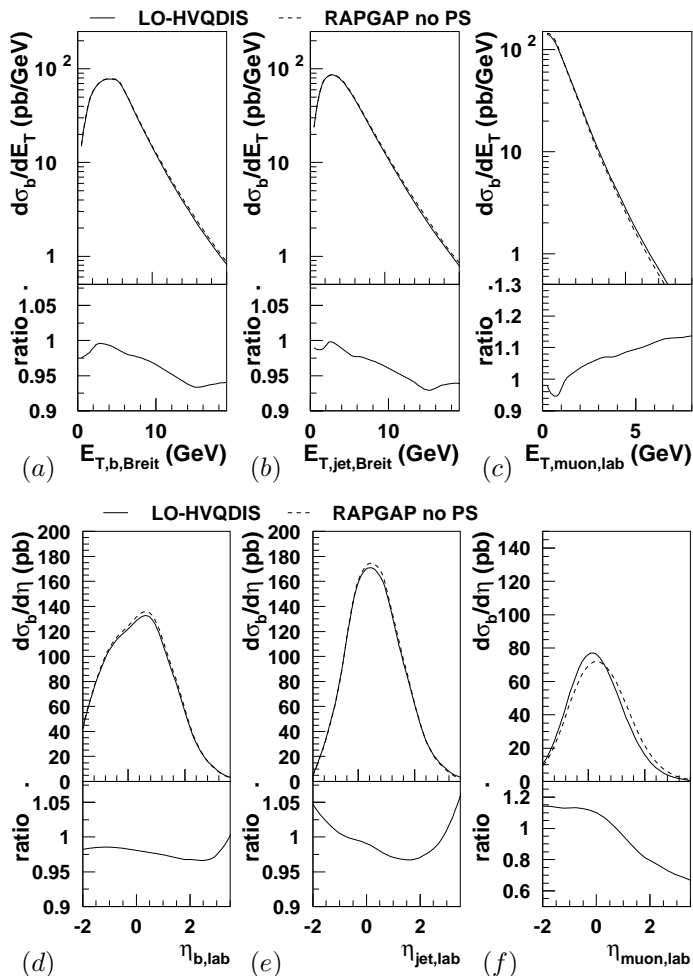


Figure 5: Inclusive DIS b -quark cross-sections as a function of (a) the transverse energy of the b -quark $E_{T,b,Breit}$, (b) the transverse energy of the jet $E_{T,jet,Breit}$, (c) the transverse energy of the muon $E_{T,\mu,lab}$, (e) the pseudo-rapidity of the jet $\eta_{jet,lab}$, (d) the pseudo-rapidity of the b -quark $\eta_{b,lab}$, (f) the pseudo-rapidity of the muon $\eta_{\mu,lab}$. Shown are LO QCD cross-section calculated by HVQDIS (LO) and by RAPGAP without parton showers. More details are given in the text.

The inclusive DIS b -quark cross-section as calculated by LO-HVQDIS is $\sigma_b = 530$ pb and agrees within 2% with the prediction from RAPGAP. For the b -quark cross-section requiring a jet $\sigma_{b,jet} = 148$ pb is found. The agreement with RAPGAP is within 4%. This is a strong indication that the LO matrix elements used in the two programs are the same. However, difference up to 5% are found for large transverse energies of the b -quark $E_{T,b,Breit}$ and of the jet $E_{T,jet,Breit}$. This can be seen in figure 5 where the inclusive b -quark cross-section σ_b as a function of the transverse energy of the b -quark $E_{T,b,Breit}$ (a) and as a function of the transverse jet energy $E_{T,jet,Breit}$ (b) in the Breit frame is shown. No strong dependence on the pseudo-rapidities of the b -quark $\eta_{b,lab}$ or of the jet pseudo-rapidities in the laboratory frame $\eta_{jet,lab}$ is found (see figures 5d and 5e).

For the b -quark cross-section requiring a jet and a muon $\sigma_{b,jet,muon} = 19$ pb is found with LO-HVQDIS, while the one from RAPGAP is 10% larger. The observed difference in $\sigma_{b,jet,muon}$ is probably due to an incomplete modeling of the muon fragmentation in the

HVQDIS program. This can be seen in figures 5c and 5f. The transverse energy spectrum of the muon is harder for the HVQDIS calculation. At large transverse energies it is 10% higher. The biggest difference is found in the pseudo-rapidity spectrum. In the RAPGAP calculation the muon is produced more forward. Difference up to 30% are found. A possible explanation of this effect is that the fragmentation model in HVQDIS is too simple to cope with the multi-parton environment where it is important that all colour connections are correctly defined.

6. Perturbative NLO QCD calculations and their uncertainties

6.1 Calculated NLO QCD cross-sections

The NLO QCD b -quark cross-sections for the four cases σ_b , $\sigma_{b,\text{jet}}$, $\sigma_{b,\text{muon}}$, $\sigma_{b,\text{jet},\text{muon}}$ are given in table 2. The cross-sections have been calculated with the renormalisation and factorisations scale set to $\mu^2 = p_{T,b}^2 + 4m_b^2$, where $p_{T,b}$ is the transverse momentum of the b -quark in the Breit or hadronic centre of mass frame.¹² The b -quark mass has been set to $m_b = 4.75$ GeV. The CTEQ5F4 parameterisation has been used for the parton densities. Also shown are the charm quark cross-sections.¹³

The inclusive charm quark cross-section is about 370 times larger than the inclusive b -quark cross-section. This is also expected, since the electrical charge of the charm quark is higher and its mass is smaller. The heavy quark mass enters directly in the matrix element and in the phase space factor, in addition it changes the parton kinematics such that different parton densities are probed. It is, however, interesting that if a hard jet or a muon is required in the detector acceptance the charm quark cross-section is only an order of magnitude bigger than the b -quark cross-section. The reason for this behaviour is that the large b -quark mass naturally produces particles at higher transverse energy.

The measurable b -quark cross-section ($\sigma_{b,\text{jet},\text{muon}}$) is about 20 times smaller than the inclusive one (σ_b). Only part of this difference is due to the branching fraction. The large fraction of the b -quark cross-section can not be measured in the detector, since the b -quark has either a low transverse energy or is produced in the forward direction¹⁴ outside the detector acceptance.

NLO	σ_b (pb)	$\sigma_{b,\text{jet}}$ (pb)	$\sigma_{b,\text{muon}}$ (pb)	$\sigma_{b,\text{jet},\text{muon}}$ (pb)
b -quark	598	230	53	26
c -quark	24170	2320	515	188

Table 2: NLO QCD cross-sections calculated for the four studied cross-section definitions for b -quarks and c -quarks.

¹²The hadronic centre of mass frame is defined as $\vec{q} + \vec{P} = 0$, where q (P) is the photon (proton) momentum. The centre of mass frame can be transformed by a longitudinal boost to the Breit frame. The transverse energy is therefore the same in both frames.

¹³The charm quark cross-section have been calculated with the factorisation and renormalisation scales set to $\mu^2 = p_{T,c}^2 + 4m_c^2$ and the charm quark mass is set to $m_c = 1.4$ GeV. The CTEQ5F3 parton density functions and the Peterson fragmentation function with $\epsilon = 0.033$ have been used. The semi-leptonic muon momentum distribution and the branching fraction $\mathcal{B}_{c \rightarrow \mu X}$ have been modified for charm quarks.

¹⁴At HERA, the proton moves into the $+z$ -direction. The forward direction is therefore the region located toward the proton remnant.

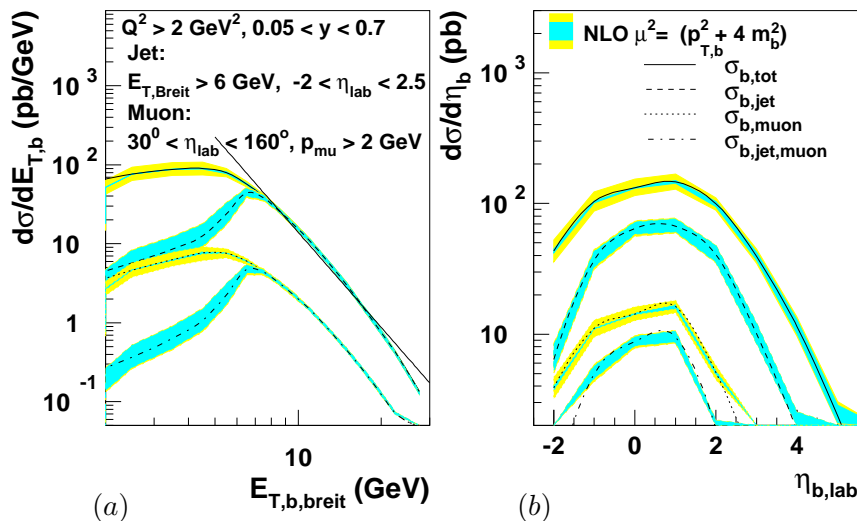


Figure 6: Cross-sections (σ_b , $\sigma_{b,jet}$, $\sigma_{b,muon}$, $\sigma_{b,jet,muon}$) as a function of the transverse energy (a) and the pseudo-rapidity of the b -quark for the four studied definition (see text). The inner band represents the renormalisation and factorisation scale uncertainties and the outer band in addition the uncertainty due to the b -quark mass. The renormalisation and factorisation scale has been set to $\mu^2 = p_{T,b}^2 + 4m_b^2$. As a comparison, the solid line indicates the power law $\sigma_b/dE_{T,b} \propto E_{T,b}^{-4}$.

The b -quark cross-section as a function of the b -quark transverse energy in the Breit frame and its pseudo-rapidity in the laboratory frame is shown in figure 6. The central NLO QCD predictions are shown as lines. The inner band indicates the renormalisation and factorisation scale uncertainties, the outer bands indicates in addition the uncertainty due to the b -quark mass. For the inclusive b -quark cross-section (σ_b) the b -quark transverse energy distribution exhibits a broad peak at about $E_{T,b,Breit} = 5$ GeV. Above this value the distribution falls like $d\sigma_b/dE_{T,b,Breit} \propto E_{T,b,Breit}^{-4}$ toward larger values. Below this value the b -quark cross-section is approximately constant. If a hard jet is required (dashed or dashed-dotted line in figure 6), the behaviour at large $E_{T,b,Breit}$ is not modified, but the region of $E_{T,b,Breit}$ is suppressed. When measuring the b -quark cross-section via the semi-leptonic muon decay, the NLO QCD predictions for relatively large $E_{T,b,Breit}$ are tested. For all shown cross-sections the uncertainties at low transverse b -quark energies are larger. Figure 6b shows the b -quark pseudo-rapidity in the laboratory frame. For all cross-section definitions most of the b -quarks are produced centrally, i.e. $-2 < \eta_{b,lab} < 2$. However, in the inclusive case (σ_b) about 10% of the b -quarks are produced at pseudo-rapidities beyond $\eta_{b,lab} > 2.5$, where there is no detector coverage. If the muon is required to be in the detector acceptance, only b -quarks within $-2 < \eta_{b,lab} < 2$ contribute to the cross-section.

6.2 Factorisation and renormalisation scale and b -quark mass uncertainties

A fixed order QCD cross-section calculation usually depends on the renormalisation and the factorisation scales. The renormalisation procedure removes divergences due to loop contributions in which virtual exchanged partons can have very large momenta (ultra-violet divergences). The factorisation scale separates the perturbatively calculable short distance

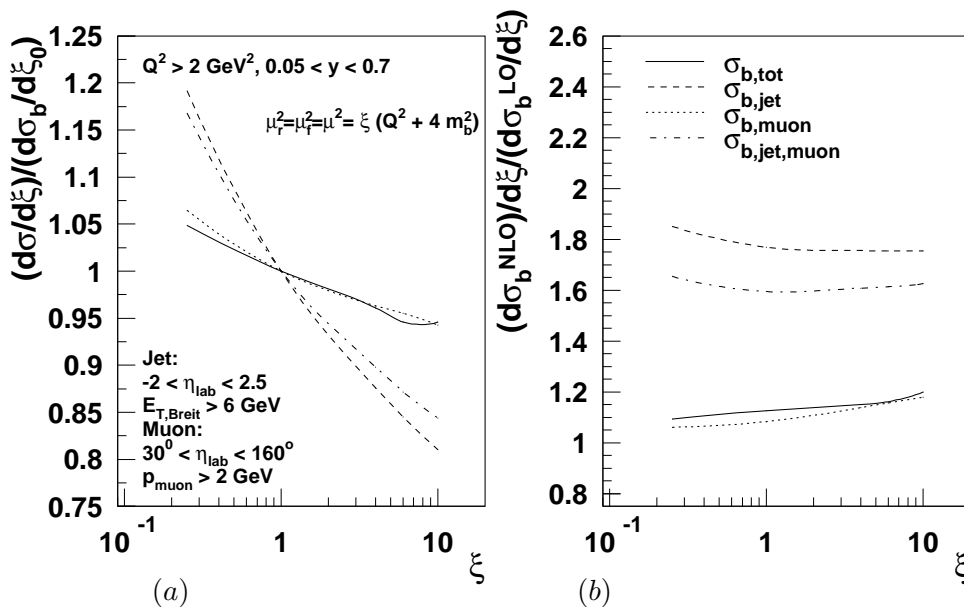


Figure 7: (a) Ratio of the cross-sections σ_b , $\sigma_{b,\text{jet}}$, $\sigma_{b,\text{muon}}$, $\sigma_{b,\text{jet,muon}}$ calculated with the renormalisation and factorisation scales set to $\mu^2 = \xi(Q^2 + 4m_b^2)$ and $\mu^2 = \xi_0(Q^2 + 4m_b^2)$ where $\xi_0 = 1$. (b) Ratio of the cross-sections calculated at NLO and at LO (K-factor) as a function of the scale factor ξ .

contributions from the non-perturbative long-distance contributions. The non-perturbative part is absorbed in the parton density functions. In this way divergences due to collinear parton radiation are removed. The choice of the renormalisation and factorisation scales in the calculation is arbitrary, but should correspond to the hard scale (Q^2) involved in the hard scattering process. In a complete calculation a physical observable does not depend on the choice of the renormalisation and factorisation scale. The residual scale dependence in a fixed order calculation can be used to estimate the uncertainties due to neglected contributions.

In a LO calculation the calculated cross-section depends on the renormalisation scale via the energy behaviour of the strong coupling $\alpha_s(\mu_r)$. When the renormalisation scale is increased, it is therefore expected that the cross-section decreases in the same way. In a NLO calculation the μ_r dependence of α_s can be compensated by the perturbatively calculable coefficient functions, since they also depend on μ_r . The scale dependence can therefore be significantly reduced when the NLO corrections are included in the calculation. In some cases the residual scale dependence is closely related to the higher order contributions which have not been calculated.

The dependence on the scale factor ξ , defined as $\mu^2 = \xi Q^2$, where Q is the hard scale, is shown in figure 7a for the four different cross-section definitions as calculated in NLO QCD. The hard scale has been chosen to be $Q^2 = Q^2 + 4m_b^2$. The cross-sections are normalised to the cross-sections obtained for $\xi = \xi_0 = 1$, i.e. the ratio $(d\sigma/d\xi)/(d\sigma/d\xi_0)$ is shown. When ξ is varied by about a factor of 10 in both directions, the inclusive cross-section σ_b varies by about $\pm 5\%$. Once a hard jet is required, the cross-section variation increases to $\pm 20\%$.

Figure 7b shows the NLO correction as a function of the scale factor ξ . The NLO correction is defined as the ratio of the cross-section calculated at NLO to the one calculated at LO. The dependence of the NLO correction on the scale factor is rather small for all studied cross-section definitions. While the NLO correction is only about 10% for the inclusive cross-section σ_b and for the one requiring a muon $\sigma_{b,\text{muon}}$, it increases to almost a factor of 2 when a jet is required.

This together with the stronger scale dependence is an indication that for the cross-section measured via the P_T^{rel} -method where a jet has to be required higher order contributions are more important. However, whenever a hard jet is involved in the cross-section measurement, the increased uncertainty is unavoidable. It is interesting that the requirement of a muon in the detector acceptance, does not lead to an increased uncertainty. This is clearly an advantage for cross-section measurements based on the B -meson lifetime using displaced vertices. However, also in this case the requirement of a hard jet in the Breit frame might be necessary in order to efficiently reject the large background from inclusive DIS events.

Here and in the following the renormalisation and factorisation scales have been set equal. Since this is an assumption with no deeper justification we have, for $Q^2 = p_{T,b}^2 + 4m_b^2$, also varied μ_r^2 and μ_f^2 independently. For all factorisation (renormalisation) scales the cross-section rises for decreasing (increasing) μ_r^2 (μ_f^2). The b -quark cross-section changes from $\sigma_b = 597.6$ pb for $\mu_f^2 = \mu_r^2 = p_{T,b}^2 + 4m_b^2$ to $\sigma_b = 671.3$ pb for $\mu_f^2 = 4(p_{T,b}^2 + 4m_b^2)$ and $\mu_r^2 = 0.25(p_{T,b}^2 + 4m_b^2)$ and to $\sigma_b = 511$ pb for $\mu_f^2 = 0.25(p_{T,b}^2 + 4m_b^2)$ and $\mu_r^2 = 4(p_{T,b}^2 + 4m_b^2)$. Similar conclusion hold for the other cross-section definitions. We find that the variation with the renormalisation scale is about equal for all choices of the factorisation scale, i.e. about $\pm 5\%$ for σ_b and about $\pm 20\%$ for $\sigma_{b,\text{jet,muon}}$. Also the dependence of the factorisation scale is about equal for all choices of the renormalisation scale, i.e. about $\pm 5\%$ for σ_b and also for $\sigma_{b,\text{jet,muon}}$. The fact that the renormalisation scale dependence does not depend on the factorisation scale choice and vice versa, remains valid even for extreme scale factors like $\xi = 40$. In the $\mu_f^2 - \mu_r^2$ plane we therefore have not found a plateau region where the scale dependence is significantly reduced with respect to other regions.

Figure 8 shows the cross-sections σ_b , $\sigma_{b,\text{jet}}$, $\sigma_{b,\text{muon}}$, $\sigma_{b,\text{jet,muon}}$ as a function of Q^2 and of $E_{T,\text{jet,Breit}}$. From $2 < Q^2 < 1000 \text{ GeV}^2$ the cross-sections fall by about 4 orders of magnitudes toward larger Q^2 (figure 8a). The Q^2 dependence is similar for all studied cross-section definitions. At low Q^2 , $\sigma_{b,\text{jet}}$ ($\sigma_{b,\text{jet,muon}}$) is about a factor 3 (2) smaller than the inclusive cross-section σ_b ($\sigma_{b,\text{muon}}$), at $Q^2 \approx 200 \text{ GeV}^2$ the ratio $\sigma_b/\sigma_{b,\text{jet}}$ ($\sigma_{b,\text{muon}}/\sigma_{b,\text{jet,muon}}$) is only 2 (1). The dependence on the transverse jet energy is similar for all cross-section definitions for $E_{T,\text{jet,Breit}} > 6 \text{ GeV}$ (see figure 8b). The inclusive cross-section σ_b as well as the one requiring a muon $\sigma_{b,\text{muon}}$ result in a mean transverse jet energy of about 10 GeV. When a hard jet is required the mean transverse jet energy increases to about 15 GeV. As a consequence possible terms of the form $\log(E_{T,\text{jet,Breit}}^2/m_b^2)$ increase from about 0.5 to 1. About 35% of the inclusive b -quark events have a hard jet with $E_{T,\text{jet,Breit}} > 6 \text{ GeV}$, when a muon in the detector acceptance is required 45% of the events have a hard jet.

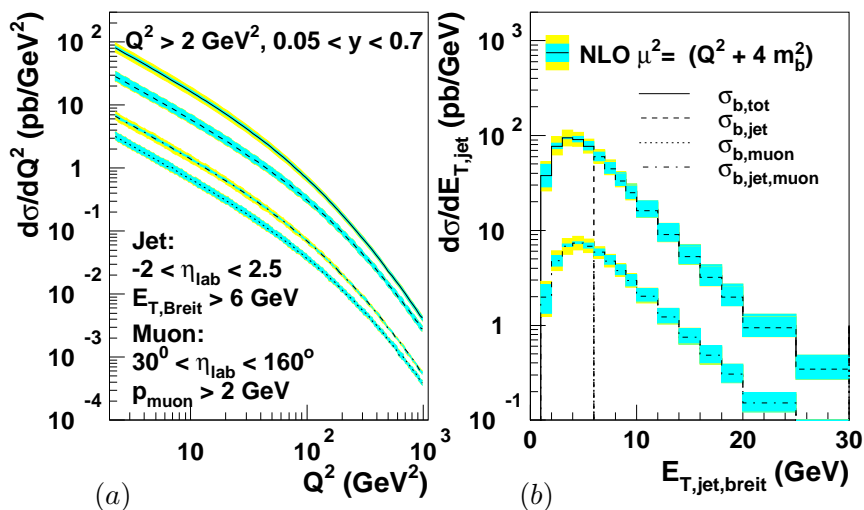


Figure 8: Cross-sections (σ_b , $\sigma_{b,jet}$, $\sigma_{b,muon}$, $\sigma_{b,jet,muon}$) as a function of Q^2 (a) and the transverse jet energy $E_{T,jet,Breit}$ (b). The inner band represents the renormalisation and factorisation scale uncertainties and the outer band in addition the uncertainty due to the b -quark mass. The renormalisation scale has been set to $\mu_r^2 = Q^2 + 4m_b^2$.

The uncertainty on the renormalisation and factorisation scales can be estimated by varying the scale factor ξ . It is common practice to vary μ^2 by approximately one order of magnitude, i.e. the scale factor is varied by $0.25 < \xi < 4$. In addition, the uncertainty introduced by the limited knowledge on the b -quark mass can be estimated by varying it between $4.5 < m_b < 5.0 \text{ GeV}$. The default value is set to $m_b = 4.75 \text{ GeV}$.

Figure 9a shows the measurable b -quark cross-section $\sigma_{b,jet,muon}$ as a function of Q^2 . The hard scale is set to $Q^2 = p_{T,b}^2 + 4m_b^2$. The inner band illustrates the scale uncertainty, the outer band shows in addition the uncertainty due to the b -quark mass. The size of the uncertainty is better visible in figure 9b where the relative difference of the modified cross-section calculation to the default cross-section calculation, i.e. $(\sigma_{b,jet,muon}(\xi_0 \pm \xi, m_b \pm \Delta m_b) - \sigma_{b,jet,muon}(\xi_0, m_b)) / \sigma_{b,jet,muon}(\xi_0, m_b)$, is shown. The total uncertainty is about $\pm 15\%$ at low Q^2 and slightly decreases towards larger Q^2 .

Also shown in figure 9a is the pure LO calculation (dashed line) and the calculation complemented with parton showers (dotted line). When parton showers are included in the calculation, the LO cross-section increases by about 15% at low Q^2 and by about 10% at large Q^2 . At low Q^2 , the NLO correction increases $\sigma_{b,jet,muon}$ by almost a factor of 2, toward larger Q^2 the NLO correction increases $\sigma_{b,jet,muon}$ by 1.6. When parton showers are included the NLO correction is lower, $\sigma_{b,jet,muon}$ increases by 1.75 at low Q^2 and by 1.5 at large Q^2 .

For b -quark production in DIS there are three possible choices for the hard scale Q^2 : m_b^2 , Q^2 and the transverse momentum of the b -quark or of the associated jet in the Breit frame. The transverse momentum can either be defined to be the transverse momentum of the b -quark $p_{T,b}$ or the maximal transverse momentum of the b -quark or the \bar{b} -quark $p_{T,b,max}$. In principle, any function of these scales is a possible choice. If one of the possible

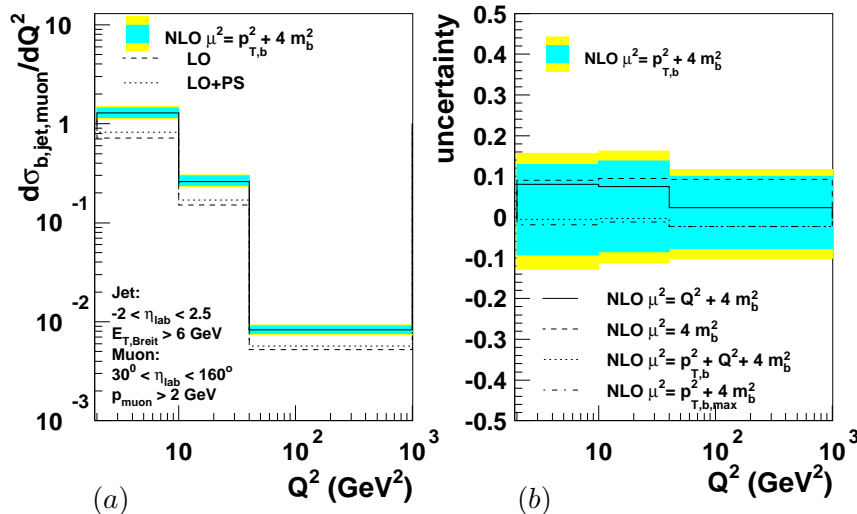


Figure 9: (a) Bottom quark cross-section $\sigma_{b,jet,muon}$ as a function of Q^2 for different choices of the renormalisation and factorisation scales μ^2 . (b) Scale uncertainty for the choice $\mu^2 = p_{T,b}^2 + 4m_b^2$ (band) and the ratio of the cross-sections when calculated with different scale choice normalised to the one calculated with $\mu^2 = p_{T,b}^2 + 4m_b^2$ (lines). The inner band represents the renormalisation and factorisation scales uncertainties and the outer band in addition the uncertainty due to the b -quark mass.

scales is much larger or smaller than the others, but still sizable, it can be expected that large logarithms of the form $\log(Q_1^2/Q_2^2)$ appear in the calculation. These logarithms have to be resummed to make the calculation reliable.

The relative difference of the cross-section calculated with different scale choices, i.e. $(\sigma_{b,jet,muon}(Q_1^2) - \sigma_{b,jet,muon}(Q_0^2))/\sigma_{b,jet,muon}(Q_0^2)$, is shown in figure 9b as a function of Q^2 . The default scale choice is $Q_0^2 = p_{T,b}^2 + 4m_b^2$. Shown as examples are $Q_1^2 = Q^2 + 4m_b^2$ (solid line), $Q_1^2 = 4m_b^2$ (dashed line), $Q_1^2 = p_{T,b}^2 + Q^2 + 4m_b^2$ (dotted line), $Q_1^2 = p_{T,b,max}^2 + 4m_b^2$ (dashed-dotted line). All studied possible scale choices lead to cross-section predictions within the uncertainties of the default choice. The choices $Q_1^2 = p_{T,b}^2 + Q^2 + 4m_b^2$ and $Q_1^2 = p_{T,b,max}^2 + 4m_b^2$ give exactly the same result. The cross-section calculated for $Q_1^2 = 4m_b^2$ is 10% higher over the full Q^2 region, the one calculated for $Q_1^2 = Q^2 + 4m_b^2$ is 10% higher at lower Q^2 , but only 2% higher at large Q^2 .

The NLO QCD cross-section prediction is therefore more or less independent on the choice of the hard scale. One way to decide which scale choice should be used as the default, is to study the uncertainties introduced by the various possible scale choice. Figure 10 shows the cross-section uncertainty for the six studied scale choices as a function of Q^2 . For all choices the total uncertainties stay within $\pm 20\%$. The uncertainty is larger at low Q^2 for all choices and decreases toward larger Q^2 . When the transverse b -quark momentum is included in the definition of Q^2 , the uncertainty is in general smaller. For instance, for $Q_1^2 = Q^2 + 4m_b^2$ the uncertainty is around $\pm(10 - 20)\%$, while for $Q_1^2 = p_{T,b}^2 + Q^2 + 4m_b^2$ the uncertainty is around $\pm(10 - 15)\%$. For $Q_1^2 = 4m_b^2$ the uncertainty is $\pm(15 - 20)\%$, while for $Q_1^2 = p_{T,b}^2 + 4m_b^2$ the uncertainty is only $\pm(10 - 15)\%$. No big difference is seen between

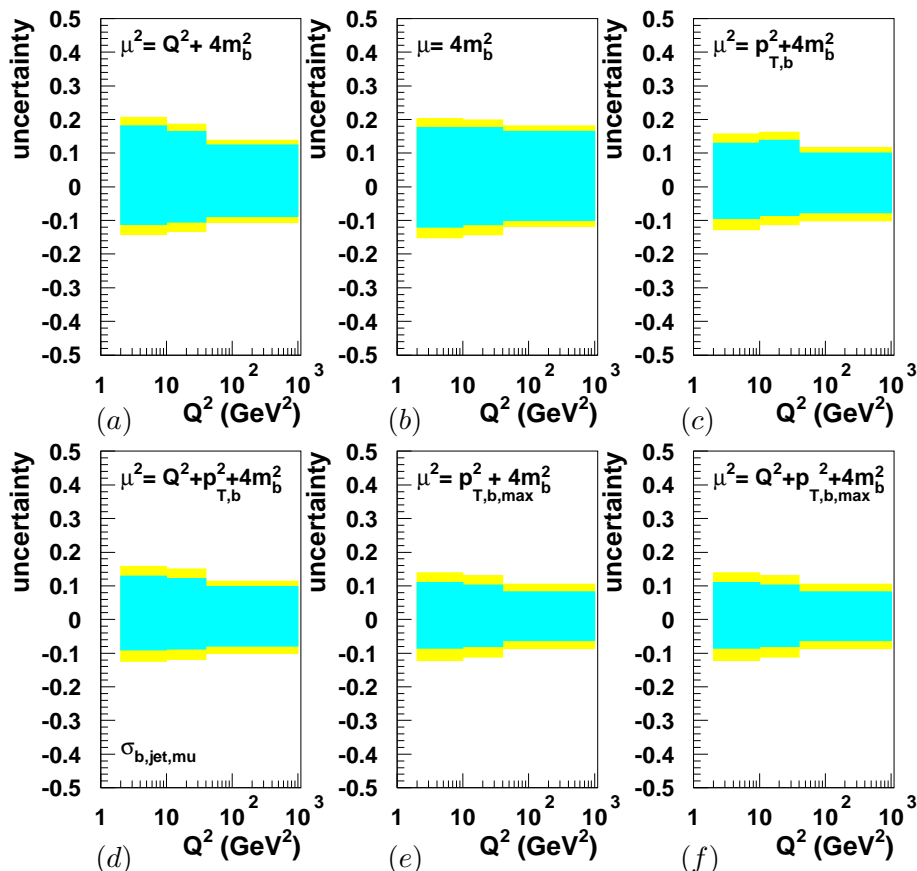


Figure 10: Uncertainty of the b -quark cross-section $\sigma_{b,\text{jet},\text{muon}}$ as a function of Q^2 for different choices of the renormalisation and factorisation scales. The inner band represents the renormalisation and factorisation scale uncertainties and the outer band in addition the uncertainty due to the b -quark mass. The scales are explained in the text.

choices involving $p_{T,b}$ or $p_{T,b,\text{max}}$. The smallest scale uncertainty is obtained for $Q_1^2 = p_{T,b}^2 + 4m_b^2$ or $Q_1^2 = p_{T,b,\text{max}}^2 + 4m_b^2$. The choice $Q_1^2 = p_{T,b}^2 + 4m_b^2$ is therefore proposed as default.

Figure 11 shows the inclusive b -quark cross-section σ_b (left) as a function of the transverse energy of the jet with the highest transverse energy ($E_{T,\text{jet},\text{Breit}}$) in the event and as a function of the pseudo-rapidity of the jet which contains the muon from the semi-leptonic b -quark decay. The scale is set to $\mu^2 = p_{T,b}^2 + 4m_b^2$. In the right part of figure 11 the uncertainty of the NLO calculation is explicitly shown. It is interesting that the scale dependence of the cross-section varies as a function of the shown observables. It is most pronounced toward larger transverse jet energies. This is the case where the transverse jet energy and consequently the transverse b -quark momentum are very different from the b -quark mass. A large scale dependence is also seen in the forward direction. For low $E_{T,\text{jet},\text{Breit}}$, where $E_{T,\text{jet},\text{Breit}} \approx m_b$, the scale dependence is rather small (down to $\pm 5\%$). This is the region where most of the inclusive b -quark events are produced. Therefore the small scale dependence of the inclusive cross-section σ_b which was discussed in the context of figure 7, seems to be purely accidental.

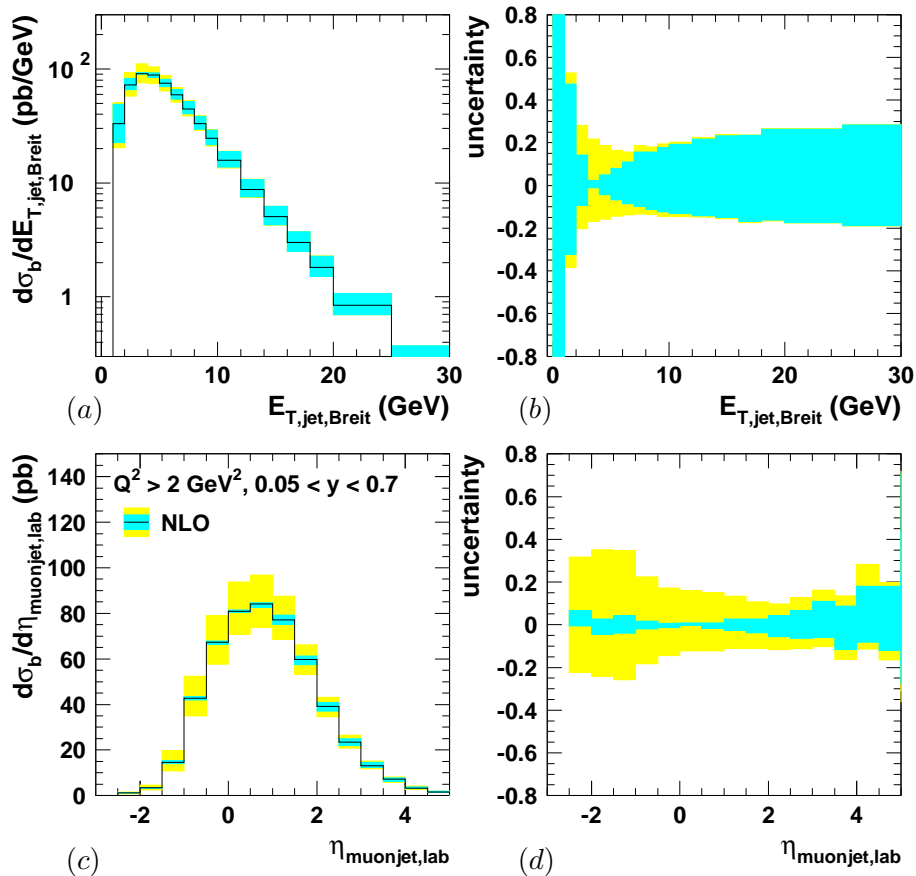


Figure 11: The cross-section σ_b as a function of the jet with the highest transverse energy $E_{T,jet,Breit}$ (a) and the pseudo-rapidity $\eta_{\mu\text{onjet,lab}}$ of the jet associated with the muon (c). The inner band represents the renormalisation and factorisation scale uncertainties and the outer band in addition the uncertainty due to the b -quark mass. The uncertainty, i.e. the ratio of the cross-section calculated with the default settings over the one with varied parameters is shown in (b) and (d). The renormalisation and factorisation scale have been set to $\mu^2 = p_{t,b}^2 + 4m_b^2$.

The total uncertainty including the b -quark mass is about constant namely around $\pm 20\%$. Only in the large $E_{T,jet,Breit}$ region the uncertainty is increased up to about 30%. In the region where the scale total uncertainty is small, the uncertainty due to the b -quark mass is large.

The increase of the uncertainties toward low $E_{T,jet,Breit}$ is most probably due to an infra-red sensitive phase space region [67, 68]. In fact, the b -quark cross-section steeply falls toward $E_{T,jet,Breit} \rightarrow 0$ and even gets slightly negative in the extreme limit (not shown). This reflects an incomplete cancellation of the (positive) divergences of the real infra-red parton emissions and the (negative) divergences of the virtual contributions. The only possibility that no hard jet is produced in the event, is the configuration where the b -quark and the \bar{b} -quark are scattered exactly in (or anti-parallel to) the direction of the proton.

Note, that the 20% total uncertainty on the inclusive cross-section σ_b is larger than the one on the $\sigma_{b,jet,muon}$ cross-section which is overall only about 15% for $\mu^2 = p_{t,b}^2 + 4m_b^2$

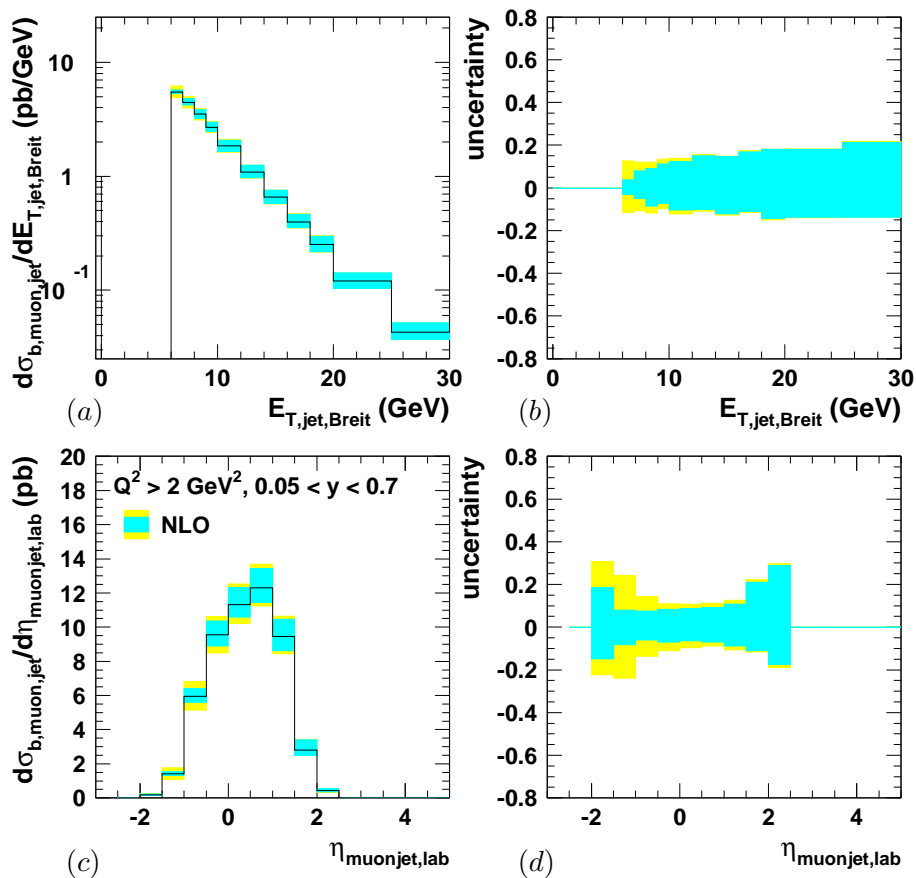


Figure 12: Same as figure 11, but for the measurable cross-section $\sigma_{b,jet,muon}$.

(see figure 10c). The differential cross-section for the case $\sigma_{b,jet,muon}$ is shown in figure 12. The uncertainties exhibit a similar behaviour than in the inclusive case, i.e. the scale dependence gets larger toward larger transverse jet energies and toward the forward region, while the b -quark mass uncertainty is largest at low transverse jet energies and in the backward region. However, the overall uncertainty is lower than in the inclusive case. At low $E_{T,jet,Breit}$, it is only about $\pm(10 - 15)\%$ and increases to about $\pm 20\%$ toward larger $E_{T,jet,Breit}$. The uncertainties in the backward and forward region toward the end of the detector acceptance are about the same in the case of σ_b and $\sigma_{b,jet,muon}$.

6.3 Parton density uncertainties

The calculation of cross-sections for observable processes generally involve the convolution of the perturbatively calculable coefficient functions corresponding to the hard subprocess with the non-perturbative parton densities which describe the structure of the proton. The parton densities absorb the collinear divergences of initial state parton radiation appearing in the perturbative calculation. The boundary defining which contributions are perturbatively calculated and which are absorbed in the parton densities is given by the factorisation scale. The parton densities can be extracted in a fit procedure by comparing cross-sections calculated by convolution them with the coefficient functions to data.

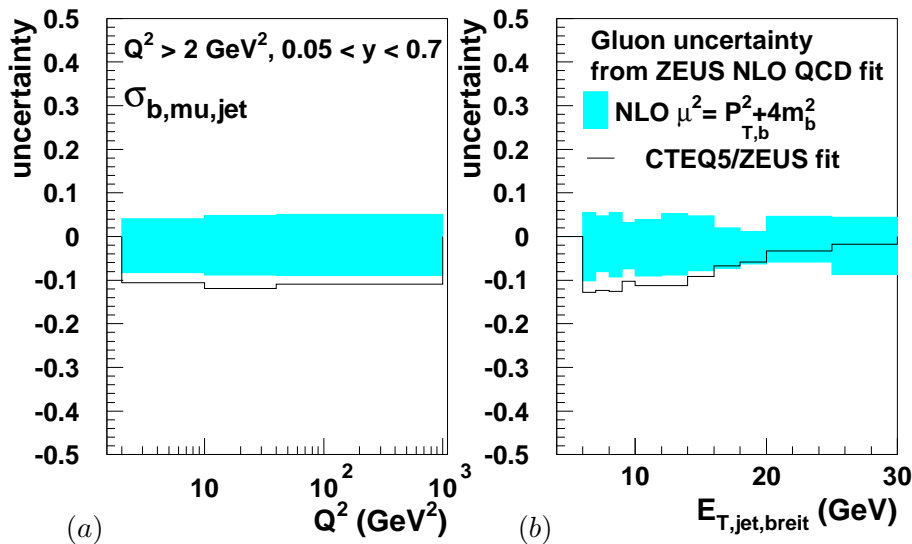


Figure 13: Uncertainty on the $\sigma_{b,\text{jet},\text{muon}}$ cross-section introduced by the uncertainty on the gluon density as a function of Q^2 (a) and $E_{T,\text{jet},\text{Breit}}$. The inner band represents the renormalisation and factorisation scale uncertainties and the outer band in addition the uncertainty due to the b -quark mass. Shown as line is the ratio of the central ZEUS NLO QCD fit and the CTEQ5F4 parameterisation.

Usually, a variety of data such as inclusive DIS, Drell-Yan, prompt photon, W -boson and inclusive jet production in ep or $p\bar{p}$ collisions etc. are used to optimally constrain the parton densities. Recently, significant progress has been made in determining in addition also the uncertainties on the parton densities. This is achieved by a careful error propagation in the fit procedure.

To estimate the impact of the limited knowledge of the proton parton densities on the calculation of the b -quark cross-section, we use the recent NLO QCD fit performed by the ZEUS collaboration [52]. Since the large part of b -quark event are initiated by gluons, the cross-section uncertainty is mainly due to the gluon density for gluon energy fractions x_g in the range¹⁵ $10^{-3} - 10^{-1}$. The hard scale where the parton densities are probed lies typically within $10 - 100 \text{ GeV}^2$.

The uncertainty of the measurable cross-section $\sigma_{b,\text{jet},\text{muon}}$ is shown as a function of Q^2 in figure 13a and as a function of $E_{T,\text{jet},\text{Breit}}$ in figure 13b. The band indicates the cross-section uncertainty due to the parton densities. The solid line gives the ratio of the cross-section calculated with the central ZEUS parton densities and the CTEQF4 parton densities. The cross-section calculated with CTEQ parameterisation is overall about 10% lower. The smaller cross-section is only observed at low $E_{T,\text{jet},\text{Breit}}$, where the bulk of the events are, for high $E_{T,\text{jet},\text{Breit}}$ the two different parton density parameterisations give about the same results. The cross-section difference is not bigger than the uncertainty determined for the ZEUS parameterisation which is not bigger than $\pm(5 - 10)\%$.

¹⁵About 90% of all b -quark events have energy fractions x_g in this range. Due to kinematic reasons, values $x_g < 10^{-3}$ can not be reached. About 10% of the events have $x_g > 10^{-1}$. In some case also very large x_g values are reached.

6.4 Fragmentation function uncertainties

The uncertainty due to the fragmentation function is estimated by changing possible choices of the fragmentation functions and their free parameters. Since care has to be taken that the fragmentation function is well matched to the perturbative calculation (see section 4.2), the estimated uncertainty is probably bigger than the real one.

Figure 14 shows the transverse energy and pseudo-rapidity distribution of the muon for the inclusive case. Shown as band is the NLO QCD cross-section σ_b calculated with the Peterson fragmentation function [58] with different parameters, i.e. $0.001 \leq \epsilon \leq 0.005$. The dashed line indicates the cross-section obtained with the parameterisation of Kartvelishvili et al. [59] using the SLD fit parameter [57] and the dotted line is obtained by using the fit parameter parameter proposed in refs. [17, 62]. While for low transverse muon energies all cross-section agree, noticeable difference are found for $E_{T,muon} \gtrsim 2$ GeV. No big differences are found in the pseudo-rapidity distribution of the muon.

Since most of the b -quark events produce muons with low transverse energies, the total measurable cross-section $\sigma_{b,jet,muon}$ varies only by about 10% when different ϵ parameters are used for the Peterson fragmentation functions and by 5% when different fragmentation functions are used.

When the b -quark cross-section σ_b is calculated in leading order, the $E_{T,muon}$ spectrum agrees with the one calculated with RAPGAP when $\epsilon = 0.009$ is used. The pseudo-rapidity distribution, however, always peaks more forward.

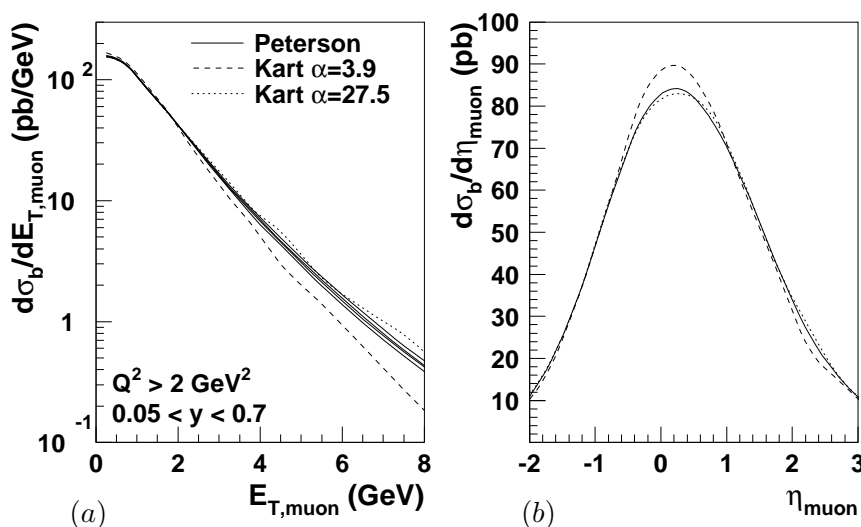


Figure 14: The b -quark cross-section σ_b as a function of the muon transverse energy (a) and pseudo-rapidity (b) calculated with different fragmentation functions. Shown as band is σ_b calculated with the Peterson fragmentation function [58] for $\epsilon = 0.001 - 0.005$ and the parameterisations of Kartvelishvili et al. [59] using the SLD fit parameter and the one obtained by a fit to the fourth moment of the b -quark fragmentation function measured in e^+e^- collisions [17, 62].

7. QCD model uncertainties

7.1 Extrapolations uncertainties due to QCD models

QCD models calculating the leading order b -quark cross-section using the leading order matrix elements and models to implement higher order radiation are the only calculations presently available that provide the full hadronic final state of an event. Therefore they are the only available tools to study the detector response and to determine the detector acceptance. Often they are also used to extrapolate from the measured cross-section to a more inclusive cross-section.

In table 3 the cross-section obtained using the QCD models is compared to the LO and NLO calculation. ME+PS denotes the parton shower model, CDM the colour dipole model and ME*+CCFM combines the off-shell matrix elements with initial parton radiation based on the CCFM evolution equations. The physics content of these QCD models is explained in more detail in section 2.

For the inclusive b -quark cross-section σ_b the same result is obtained for the ME+PS and for the CDM model. Since the inclusive cross-section does not depend on the treatment of the hadronic final state this is also expected. It is, however, interesting that the b -quark cross-section requiring a jet or a muon in the final state, are also very similar for both models. The inclusive cross-section σ_b is 25% lower than the NLO QCD result. This difference between the QCD model and the NLO QCD calculation increases to about 40% when a jet or a muon is required in the cross-section definition. While for σ_b the QCD models agree with the LO QCD calculation, they lead to a 20% – 40% bigger cross-section, when a jet is required. The increase is due to the inclusion of the parton showers.

Since in the ME*+CCFM model a different gluon density in addition to the different parton radiation pattern and the off-shell matrix elements is used, the inclusive b -quark calculated cross-section can be different. The ME*+CCFM model gives a cross-section which is 2 – 3 times higher than the one calculated with the ME+PS or CDM models and about 20% – 40% higher than the NLO QCD result.

When the QCD models are used to remove the jet in the cross-section definition, i.e

Model	σ_b (pb)	$\sigma_{b,jet}$ (pb)	$\sigma_{b,muon}$ (pb)	$\sigma_{b,jet,muon}$ (pb)
NLO	597.6	230.4	52.7	26.1
LO	449.4	113.6	40.8	14.4
ME+PS	475.2	164.7	38.7	17.1
ME only	475.2	123.3	38.5	13.8
CDM	475.2	163.5	37.0	16.3
ME*+CCFM	822.0	364.4	65.8	35.5

Table 3: Calculated b -quark cross-sections for the four studied definitions. The calculations are made with $\mu^2 = p_{T,b}^2 + 4m_b^2$. See the text for more explanations.

quoting $\sigma_{b,\text{muon}}$ instead of $\sigma_{b,\text{jet},\text{muon}}$, the following extrapolation factor has to be calculated:

$$\sigma_b^{\text{data}} = \sigma_{b,\text{jet},\text{muon}}^{\text{data}} \cdot \frac{\sigma_b^{\text{MC}}}{\sigma_{b,\text{jet},\text{muon}}^{\text{MC}}}.$$

For MEPS and CDM this extrapolation factor is about 2.3. However, for NLO it is only 2.0 and for ME*+CCFM it is 1.8. Since it is not known, which of the calculation gives the correct result, the jet extrapolation introduces a model uncertainty of about 20%. If one, for instance, assumed that the experimental measurement would give $\sigma_{b,\text{jet},\text{muon}} = 35.5$ pb as predicted by CASCADE and one used the MEPS Monte Carlo simulation to quote a cross-section $\sigma_{b,\text{muon}}$, the result would be $\sigma_{b,\text{muon}} = 78.1$ pb. This is, however, about 20% higher than the correct result. Moreover, the extrapolation factor is dependent on the choice of the renormalisation and factorisation scales. This is illustrated for the NLO QCD calculation in figure 7. The ratio of the dashed-dotted and the dotted line is the extrapolation factor needed to correct for the jet acceptance. The extrapolation factor varies from 1.8 obtained for scale choice of $\xi = 0.1$ to 2.25 for $\xi = 10$, which corresponds to a change by 20%.

Sometimes the jet definition is kept in the cross-section definition, but the requirement of a muon is removed in order to get a cross-section definition where no fragmentation model is involved in the NLO QCD cross-section calculation. The idea of such a procedure is that the complex fragmentation model as implemented in the QCD models are more reliable than the very simple one used in the NLO QCD calculation.¹⁶ If the muon requirement is removed from the cross-section definition, the following extrapolation factor has to be calculated:

$$\sigma_{b,\text{jet}}^{\text{data}} = \sigma_{b,\text{jet},\text{muon}}^{\text{data}} \cdot \frac{\sigma_{b,\text{jet}}^{\text{MC}}}{\sigma_{b,\text{jet},\text{muon}}^{\text{MC}}}$$

The correction factor calculated with MEPS, CDM or ME*+CCFM is about 10. The one calculated with NLO QCD is 8.8. The introduced model uncertainty is about 10%. The correction factor is rather large, only 10% of the quoted cross-section result is actually measured in the detector. However, part of the correction is due to the muon branching fraction which is well known. About 75% of the muon in the rapidity range measured by the detector $-1.7 < \eta_{\text{muon}} < 1.3$ and about 30% of the muons satisfy $p_{\text{muon}} > 2$ GeV.

The model uncertainties of the extrapolation factors are related to the different distribution of the variables defining the cross-section, i.e. the muon and jet transverse energies and pseudo-rapidities. The shapes of these distributions for inclusive b -quark events are shown in figure 15. Figure 15a shows the transverse energy of the jet with the highest E_T in the Breit frame and figure 15b shows the pseudo-rapidity of the jet which is associated with the muon.¹⁷ Figure 15c and figure 15d show the transverse energy and the pseudo-rapidity of the muon. Given the very different treatments of the underlying partonic final

¹⁶Even if this idea sounds reasonable one has to be careful, since the different partonic final state can lead to different distributions of the variables defining the muon kinematics.

¹⁷The association of the muon and the jet is performed by the jet algorithm.

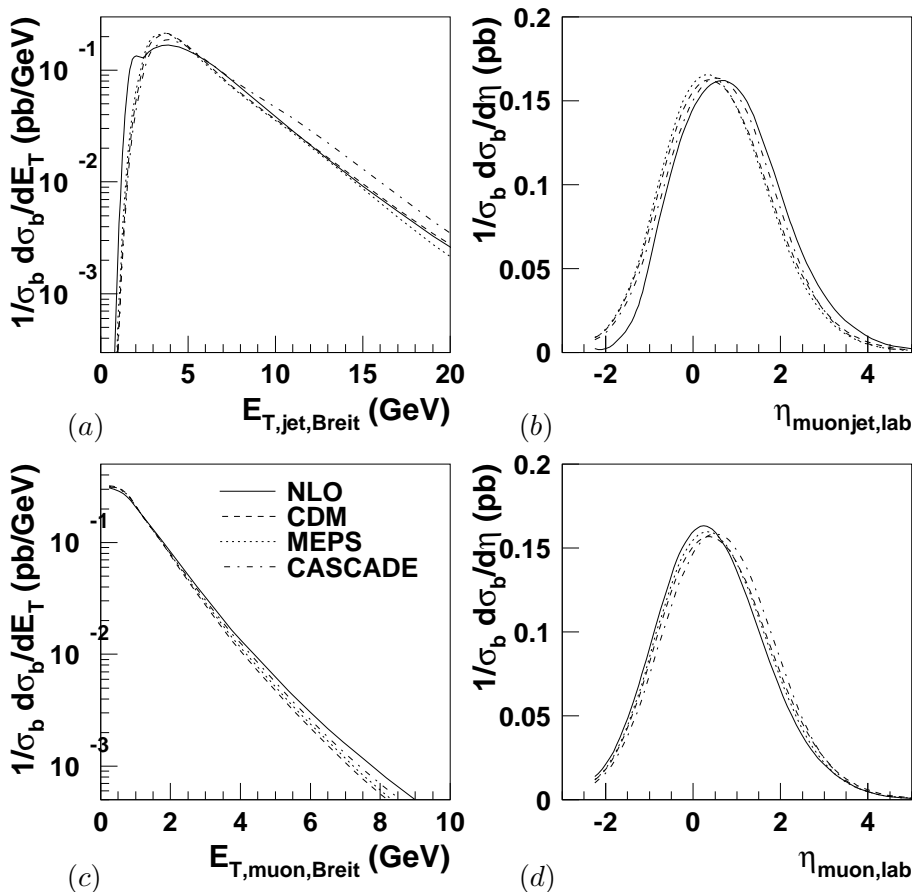


Figure 15: Comparison of the shape of the transverse energy and the pseudo-rapidity distribution of the jet and the muon for the inclusive b -quark cross-section as obtained by the NLO QCD calculation and the QCD Monte Carlo models.

state it is remarkable that the jet and muon distribution of the tested calculations are not too different.

The CDM and NLO QCD have a similar transverse jet energy spectrum. The MEPS model produces less events at high E_T . The spectrum calculated by ME^*+CCFM is significantly harder. Less events at low E_T and more events at large E_T are expected. The pseudo-rapidity spectrum of the jet associated to the muon is similar for the MEPS and the CDM model. NLO QCD has a spectrum which is clearly shifted toward the forward direction. In between these two models lies the ME^*+CCFM prediction. In contrast to the transverse jet energy NLO QCD exhibits the hardest transverse muon energy spectrum. MEPS and CDM have similar spectra. ME^*+CCFM lies in between. At low transverse muon energies all calculations more or less agree. The muon pseudo-rapidity spectrum is most shifted toward the forward region for the ME^*+CCFM prediction. NLO QCD is most backward and CDM agrees more or less with MEPS.

The detailed understanding of these distributions is rather difficult. While the jet distributions are a reflection of the different partonic final state, the muon distributions also include hadronisation effects. It is e.g. remarkable that the muon pseudo-rapidity distribu-

tion is most shifted toward the backward region for the NLO QCD calculation, although the jet pseudo-rapidity distribution is shifted most forward. This might be explained by the observation made in the context of figure 5 that the hadronisation pulls the muon forward.

7.2 Hadronisation corrections uncertainties

If a jet is required in the cross-section calculation, the NLO QCD prediction should be corrected for hadronisation effects, since the jets can only be formed by the three partons available in the final state. Such a correction is, however, only meaningful, if the shape of the transverse energy and pseudo-rapidity distributions of the parton jets calculated with the QCD models is not too different from the one of the NLO QCD calculation.

The cross-section $\sigma_{b,\text{jet},\mu\text{on}}$ decreases by about 10% at low Q^2 and by about 5% at high Q^2 , if hadronisation effects are included. The dependence of the hadronisation corrections on the transverse jet energy and the jet pseudo-rapidity for the cross-section $\sigma_{b,\text{jet},\mu\text{on}}$ is shown in figure 16a and figure 16c. The solid line is the MEPS expectation based on the hadronic final state, the dashed line is the one based on the partonic final state. Hadronisation effects lower the cross-section at low E_T , but increase the cross-section

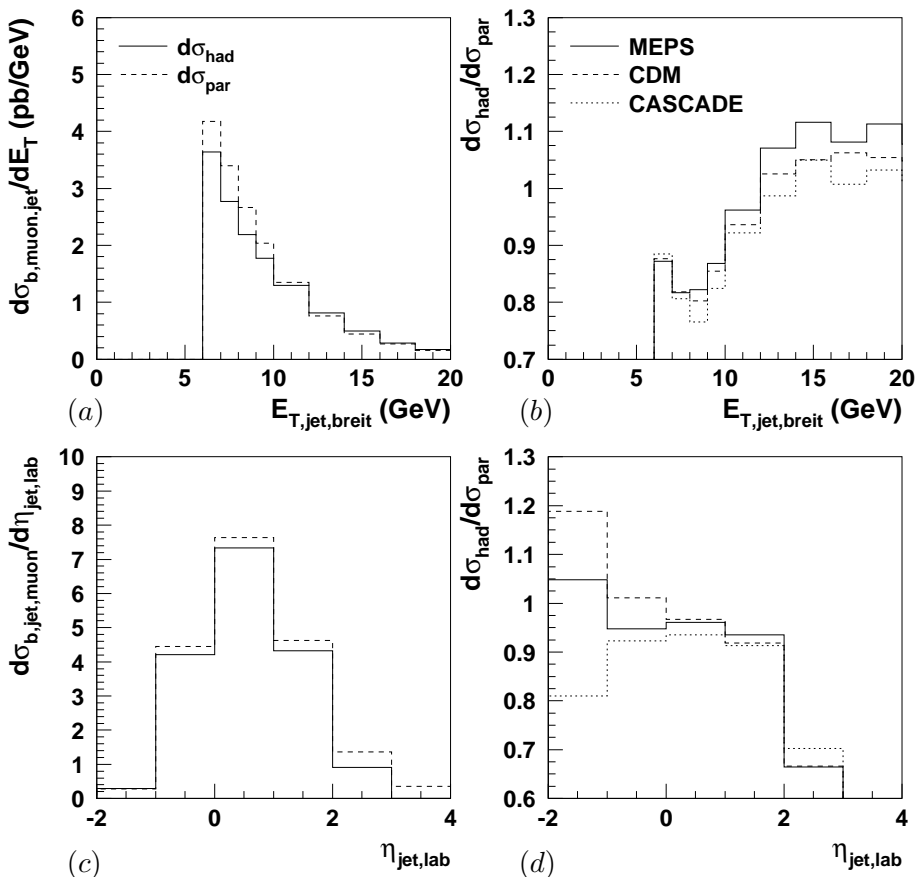


Figure 16: Transverse jet energy and pseudo-rapidity for the measurable cross-section $\sigma_{b,\text{jet},\mu\text{on}}$ based on the hadronic (σ_{had}) and the partonic (σ_{par}) final state.

at high E_T . The hadronisation correction factor, i.e. $\sigma_{\text{had}}/\sigma_{\text{par}}$ is shown in figure 16b and figure 16d for the three discussed QCD models. The symbol σ_{had} denotes the b -quark cross-section calculated for hadrons, σ_{par} denotes the b -quark cross-section calculated for partons. The biggest model uncertainties on the hadronisation correction is seen at large transverse jet energies and for low jet pseudo-rapidities. This are, however, the regions where the cross-section is rather small.

8. Conclusions

The uncertainties involved in the NLO QCD calculation of b -quark cross-sections have been estimated. Besides the inclusive b -quark cross-section, cross-section definition requiring the muon from the semi-leptonic b -quark decay or the jet induced by the b -quark have been studied. The uncertainties due to the renormalisation and factorisation scale are about 10% – 20%. The uncertainties introduced by possible scale choices are within this margin. In general, the total uncertainties including the uncertainties on the b -quark mass are about constant over the full jet transverse energy and pseudo-rapidity range. The total uncertainties are smallest for the cross-section where the muon and the jet are within the detector acceptance. When extrapolating the measurable cross-section to more inclusive cross-section definitions large extrapolation factors can be involved. The model uncertainties on these factors are estimated to be 20%. Hadronisation corrections lead to model uncertainties of about 10%.

Acknowledgments

We would like to thank M. Cacciari, H. Jung and M. Corradi for the fruitful comments and critical reading of the manuscript.

References

- [1] UA1 collaboration, C. Albajar et al., *Beauty production at the CERN $p\bar{p}$ collider*, *Phys. Lett.* **B 256** (1991) 121.
- [2] CDF collaboration, F. Abe et al., *Measurement of the bottom quark production cross-section using semileptonic decay electrons in $p\bar{p}$ collisions at $\sqrt{s} = 1.8$ TeV*, *Phys. Rev. Lett.* **71** (1993) 500.
- [3] CDF collaboration, F. Abe et al., *Measurement of bottom quark production in 1.8-TeV $p\bar{p}$ collisions using semileptonic decay muons*, *Phys. Rev. Lett.* **71** (1993) 2396.
- [4] CDF collaboration, F. Abe et al., *Measurement of correlated μ -anti- b jet cross-sections in $p\bar{p}$ collisions at $\sqrt{s} = 1.8$ TeV*, *Phys. Rev.* **D 53** (1996) 1051 [[hep-ex/9508017](#)].
- [5] CDF collaboration, F. Abe et al., *Measurement of b anti- b production correlations, B_0 anti- B_0 mixing and a limit on $\epsilon(b)$ in $p\bar{p}$ collisions at $\sqrt{s} = 1.8$ TeV*, *Phys. Rev.* **D 55** (1997) 2546.
- [6] D0 collaboration, S. Abachi et al., *Inclusive mu and b quark production cross-sections in $p\bar{p}$ collisions at $\sqrt{s} = 1.8$ TeV*, *Phys. Rev. Lett.* **74** (1995) 3548.

- [7] D0 collaboration, S. Abachi et al., *J/ψ production in p \bar{p} collisions at $\sqrt{s} = 1.8$ TeV*, *Phys. Lett. B* **370** (1996) 239.
- [8] D0 collaboration, B. Abbott et al., *The b anti-b production cross section and angular correlations in p \bar{p} collisions at $\sqrt{s} = 1.8$ TeV*, *Phys. Lett. B* **487** (2000) 264 [[hep-ex/9905024](#)].
- [9] L3 collaboration, M. Acciarri et al., *Measurements of the cross sections for open charm and beauty production in $\gamma\gamma$ collisions at $\sqrt{s} = 189$ GeV - 202-GeV*, *Phys. Lett. B* **503** (2001) 10 [[hep-ex/0011070](#)].
- [10] H1 collaboration, C. Adloff et al., *Measurement of open beauty production at HERA*, *Phys. Lett. B* **467** (1999) 156 [[hep-ex/9909029](#)].
- [11] ZEUS collaboration, J. Breitweg et al., *Measurement of open beauty production in photoproduction at HERA*, *Eur. Phys. J. C* **18** (2001) 625 [[hep-ex/0011081](#)].
- [12] M. Cacciari, M. Greco and P. Nason, *The p_T spectrum in heavy-flavour hadroproduction*, *J. High Energy Phys.* **05** (1998) 007 [[hep-ph/9803400](#)].
- [13] R.D. Ball and R.K. Ellis, *Heavy quark production at high energy*, *J. High Energy Phys.* **05** (2001) 053 [[hep-ph/0101199](#)].
- [14] H. Jung, *Heavy quark production at the Tevatron and HERA using k_t factorization with CCFM evolution*, *Phys. Rev. D* **65** (2002) 034015 [[hep-ph/0110034](#)].
- [15] P. Hagler, R. Kirschner, A. Schafer, L. Szymanowski and O. Teryaev, *Heavy quark hadroproduction as a test of the effective BFKL q anti-q vertex*, *Phys. Rev. D* **62** (2000) 071502 [[hep-ph/0002077](#)].
- [16] A.V. Lipatov, V.A. Saleev and N.P. Zotov, *Heavy quark production at the Tevatron in the semihard QCD approach and the unintegrated gluon distribution*, [hep-ph/0112114](#).
- [17] M. Cacciari and P. Nason, *Is there a significant excess in bottom hadroproduction at the Tevatron?*, *Phys. Rev. Lett.* **89** (2002) 122003 [[hep-ph/0204025](#)].
- [18] E.L. Berger et al., *Low energy supersymmetry and the Tevatron bottom-quark cross section*, *Phys. Rev. Lett.* **86** (2001) 4231 [[hep-ph/0012001](#)].
- [19] P. Janot, *The light gluino mass window revisited*, *Phys. Lett. B* **564** (2003) 183 [[hep-ph/0302076](#)].
- [20] W.L. van Neerven, *Production of heavy quarks in deep inelastic lepton hadron scattering*, [hep-ph/0107193](#).
- [21] B.W. Harris and J. Smith, *Charm quark and $D^{*,\pm}$ cross sections in deeply inelastic scattering at HERA*, *Phys. Rev. D* **57** (1998) 2806 [[hep-ph/9706334](#)].
- [22] B.W. Harris and J. Smith, *Heavy quark correlations in deep inelastic electroproduction*, *Nucl. Phys. B* **452** (1995) 109 [[hep-ph/9503484](#)].
- [23] B.W. Harris and J. Smith, *Invariant mass distributions for heavy quark-anti-quark pairs in deep inelastic electroproduction*, *Phys. Lett. B* **353** (1995) 535 [[hep-ph/9502312](#)].
- [24] H. Jung, *Hard diffractive scattering in high-energy e p collisions and the Monte Carlo generation RAPGAP*, *Comp. Phys. Commun.* **86** (1995) 147–161.
- [25] M. Bengtsson and T. Sjostrand, *Parton showers in leptoproduction events*, *Z. Physik C* **37** (1988) 465.

- [26] V.N. Gribov and L.N. Lipatov, *Deep inelastic ep scattering in perturbation theory*, *Yad. Fiz.* **15** (1972) 781.
- [27] G. Altarelli and G. Parisi, *Asymptotic freedom in parton language*, *Nucl. Phys.* **B 126** (1977) 298.
- [28] Y.L. Dokshitzer, *Calculation of the structure functions for deep inelastic scattering and e^+e^- annihilation by perturbation theory in quantum chromodynamics. (in russian)*, *Sov. Phys. JETP* **46** (1977) 641.
- [29] B. Andersson, G. Gustafson, G. Ingelman and T. Sjostrand, *Parton fragmentation and string dynamics*, *Phys. Rept.* **97** (1983) 31.
- [30] T. Sjostrand, *High-energy physics event generation with Pythia 5.7 and Jetset 7.4*, *Comput. Phys. Commun.* **82** (1994) 74.
- [31] L. Lonnblad, *Ariadne version 4: a program for simulation of QCD cascades implementing the color dipole model*, *Comput. Phys. Commun.* **71** (1992) 15.
- [32] G. Gustafson and U. Pettersson, *Dipole formulation of QCD cascades*, *Nucl. Phys.* **B 306** (1988) 746.
- [33] B. Andersson, G. Gustafson, L. Lonnblad and U. Pettersson, *Coherence effects in deep inelastic scattering*, *Z. Physik* **C 43** (1989) 625.
- [34] H. Jung, *The CCFM Monte Carlo generator CASCADE*, *Comput. Phys. Commun.* **143** (2002) 100 [[hep-ph/0109102](#)].
- [35] M. Ciafaloni, *Coherence effects in initial jets at small Q^2/s* , *Nucl. Phys.* **B 296** (1988) 49.
- [36] S. Catani, F. Fiorani and G. Marchesini, *QCD coherence in initial state radiation*, *Phys. Lett.* **B 234** (1990) 339.
- [37] S. Catani, F. Fiorani and G. Marchesini, *Small x behavior of initial state radiation in perturbative QCD*, *Nucl. Phys.* **B 336** (1990) 18.
- [38] G. Marchesini, *QCD coherence in the structure function and associated distributions at small x* , *Nucl. Phys.* **B 445** (1995) 49 [[hep-ph/9412327](#)].
- [39] E. Laenen, S. Riemersma, J. Smith and W.L. van Neerven, *$\mathcal{O}(\alpha_s)$ corrections to heavy flavor inclusive distributions in electroproduction*, *Nucl. Phys.* **B 392** (1993) 229.
- [40] E. Laenen, S. Riemersma, J. Smith and W.L. van Neerven, *Complete $\mathcal{O}(\alpha_s)$ corrections to heavy flavor structure functions in electroproduction*, *Nucl. Phys.* **B 392** (1993) 162.
- [41] E. Laenen and S. Riemersma, *Heavy-quark production in $e\gamma$ scattering*, *Phys. Lett.* **B 376** (1996) 169 [[hep-ph/9602258](#)].
- [42] G.A. Schuler, *Heavy flavor production at HERA*, *Nucl. Phys.* **B 299** (1988) 21.
- [43] E.A. Kuraev, L.N. Lipatov and V.S. Fadin, *Multi-reggeon processes in the Yang-Mills theory*, *Sov. Phys. JETP* **44** (1976) 443.
- [44] E.A. Kuraev, L.N. Lipatov and V.S. Fadin, *The Pomernanchuk singularity in nonabelian gauge theories*, *Sov. Phys. JETP* **45** (1977) 199.
- [45] I.I. Balitsky and L.N. Lipatov, *The Pomernanchuk singularity in quantum chromodynamics*, *Sov. J. Nucl. Phys.* **28** (1978) 822.

- [46] S. Catani, M. Ciafaloni and F. Hautmann, *High-energy factorization and small x heavy flavor production*, *Nucl. Phys. B* **366** (1991) 135.
- [47] H1 collaboration, S. Aid et al., *A measurement and QCD analysis of the proton structure function $F_2(x, Q^2)$ at HERA*, *Nucl. Phys. B* **470** (1996) 3 [[hep-ex/9603004](#)].
- [48] S.D. Ellis and D.E. Soper, *Successive combination jet algorithm for hadron collisions*, *Phys. Rev. D* **48** (1993) 3160 [[hep-ph/9305266](#)].
- [49] S. Catani, Y.L. Dokshitzer, M.H. Seymour and B.R. Webber, *Longitudinally invariant k_t clustering algorithms for hadron hadron collisions*, *Nucl. Phys. B* **406** (1993) 187.
- [50] M.H. Seymour, *Jet shapes in hadron collisions: higher orders, resummation and hadronization*, *Nucl. Phys. B* **513** (1998) 269 [[hep-ph/9707338](#)].
- [51] CTEQ collaboration, H.L. Lai et al., *Global QCD analysis of parton structure of the nucleon: CTEQ5 parton distributions*, *Eur. Phys. J. C* **12** (2000) 375 [[hep-ph/9903282](#)].
- [52] ZEUS collaboration, S. Chekanov et al., *A ZEUS next-to-leading-order QCD analysis of data on deep inelastic scattering*, *Phys. Rev. D* **67** (2003) 012007 [[hep-ex/0208023](#)].
- [53] ALEPH collaboration, D. Buskulic et al., *Measurement of the effective b quark fragmentation function at the z resonance*, *Phys. Lett. B* **357** (1995) 699.
- [54] OPAL collaboration, G. Alexander et al., *A study of b quark fragmentation into B^0 and B^+ mesons at LEP*, *Phys. Lett. B* **364** (1995) 93.
- [55] ALEPH collaboration, A. Heister et al., *Study of the fragmentation of b quarks into B -mesons at the Z peak*, *Phys. Lett. B* **512** (2001) 30 [[hep-ex/0106051](#)].
- [56] OPAL collaboration, G. Abbiendi et al., *Inclusive analysis of the b quark fragmentation function in Z decays at LEP*, [hep-ex/0210031](#).
- [57] SLD collaboration, K. Abe et al., *Measurement of the b -quark fragmentation function in Z^0 decays*, *Phys. Rev. D* **65** (2002) 092006 [[hep-ex/0202031](#)].
- [58] C. Peterson, D. Schlatter, I. Schmitt and P.M. Zerwas, *Scaling violations in inclusive e^+e^- annihilation spectra*, *Phys. Rev. D* **27** (1983) 105.
- [59] V.G. Kartvelishvili, A.K. Likhoded and V.A. Petrov, *On the fragmentation functions of heavy quarks into hadrons*, *Phys. Lett. B* **78** (1978) 615.
- [60] B. Mele and P. Nason, *The fragmentation function for heavy quarks in QCD*, *Nucl. Phys. B* **361** (1991) 626.
- [61] M. Cacciari and M. Greco, *Large p_T hadroproduction of heavy quarks*, *Nucl. Phys. B* **421** (1994) 530 [[hep-ph/9311260](#)].
- [62] M. Cacciari, *Perturbative and non-perturbative issues in heavy quark fragmentation*, [hep-ph/0205326](#).
- [63] R.L. Jaffe and L. Randall, *Heavy quark fragmentation into heavy mesons*, *Nucl. Phys. B* **412** (1994) 79 [[hep-ph/9306201](#)].
- [64] P. Nason and B.R. Webber, *Non-perturbative corrections to heavy quark fragmentation in e^+e^- annihilation*, *Phys. Lett. B* **395** (1997) 355 [[hep-ph/9612353](#)].
- [65] M. Cacciari and E. Gardi, *Heavy-quark fragmentation*, *Nucl. Phys. B* **664** (2003) 299 [[hep-ph/0301047](#)].

- [66] PARTICLE DATA GROUP collaboration, K. Hagiwara et al., *Review of particle physics*, *Phys. Rev. D* **66** (2002) 010001.
- [67] S. Frixione and G. Ridolfi, *Jet photoproduction at HERA*, *Nucl. Phys. B* **507** (1997) 315 [[hep-ph/9707345](#)].
- [68] S. Catani and B.R. Webber, *Infrared safe but infinite: soft-gluon divergences inside the physical region*, *J. High Energy Phys.* **10** (1997) 005 [[hep-ph/9710333](#)].